forests

MDPI

Article

Multi-Hydrological Factor-Driven Attribution and Future Prediction of Vegetation Dynamics on the Qinghai-Tibetan Plateau

Qiang Meng [1,2], Qiang He [1,2,*], Wenxin Yang [3], Peng Chen [4,*], Jingxia Liu [1,2], Zhaoqiang Zhou [4] and Xiaowen Wang [5,6]

1 College of Water Conservancy and Civil Engineering, Xizang Agricultural and Animal Husbandry University, Linzhi 860000, China; mengqiang@xza.edu.cn (Q.M.)
2 Plateau Water Environment and Water Ecology Laboratory, Xizang Agriculture and Animal Husbandry University, Linzhi 860000, China
3 College of Hydraulic and Civil Engineering, Xinjiang Agricultural University, Urumqi 830052, China
4 College of Hydraulic Science and Engineering, Northeast Agricultural University, Harbin 150030, China
5 High-Tech Key Laboratory of Agricultural Equipment and Intelligence of Jiangsu Province, Jiangsu University, Zhenjiang 212013, China
6 School of Agricultural Engineering, Jiangsu University, Zhenjiang 212013, China
* Correspondence: hqiang@xza.edu.cn (Q.H.); chenpeng_isotope@163.com (P.C.)

Abstract

Accurately assessing and predicting vegetation dynamics is of great significance for evaluating regional hydrological and ecological environments. This study focuses on the climate-sensitive Qinghai-Tibetan Plateau (QTP), aiming to reveal the spatiotemporal patterns, underlying driving mechanisms, and future trends of vegetation dynamics. The historical turning points of greening trends were identified using the running slope difference method, and the SHapley Additive exPlanations (SHAP) method was employed to analyze the key driving factors. An Xtreme Gradient Boosting (XGBoost) prediction model was constructed and validated, and then coupled with Coupled Model Intercomparison Project Phase 6 (CMIP6) multi-model ensemble data to project seasonal vegetation changes under different Shared Socioeconomic Pathways (SSP). The main conclusions are as follows: (1) Vegetation on the QTP showed an overall greening trend with significant spatial heterogeneity. Approximately 47.25% of the area exhibited no trend shift (NS), while 29.42% experienced a shift from greening to browning (GB), with most shifts occurring between 1990 and 2010. (2) Soil moisture and precipitation were the dominant driving factors, with contributions significantly higher than those of temperature, wind speed, and other variables, and they exhibited nonlinear interactive effects with the Normalized Difference Vegetation Index (NDVI). (3) In the future, vegetation is projected to show an overall increasing trend, with stronger responses in spring and autumn. The regional average rate of change is highest in spring, especially under the SSP5-8.5 scenario (17.8% for 2030–2060 and 26.4% for 2061–2100); in autumn, although the regional average rate of change is small, the internal spatial variability is significant. The humid regions in the eastern and southeastern parts of the QTP demonstrated more active greening across all seasons except winter, and high-emission scenarios are expected to exacerbate regional and seasonal differences. This study systematically reveals the adaptive dynamics and future scenarios of vegetation dynamics on the QTP, providing scientific support for the adaptation of alpine ecosystems to global change and the management of regional ecological security barriers.

Check for updates

Academic Editor: Xiaochun Wang

Received: 1 April 2026
Revised: 13 May 2026
Accepted: 28 May 2026
Published: 31 May 2026

Copyright: © 2026 by the authors. Licensee MDPI, Basel, Switzerland. This article is an open access article distributed under the terms and conditions of the Creative Commons Attribution (CC BY) license.

Keywords: NDVI; CMIP6; Tibetan Plateau; SHAP; XGBoost

1. Introduction

Vegetation plays an irreplaceable role in regulating water and carbon cycles, serving as a key component of terrestrial ecosystems [1]. There exists a complex mutual feedback relationship between ecosystems and hydrological processes [2,3]. Hydrological processes encompass several core elements, such as precipitation, evapotranspiration, temperature, and soil moisture, while ecosystems are coupled with hydrological processes primarily through physiological mechanisms such as plant transpiration [4,5] and root water uptake [6]. Deepening our understanding of this interactive mechanism carries major scientific significance and practical value. It supports efforts to combat climate change, reduce greenhouse gas emissions, optimize water resource management, and protect ecological security.

The Qinghai-Tibetan Plateau (QTP) is one of the typical and critical areas sensitive to the impacts of global climate change [7]. Although the region possesses abundant total water resources, their spatial and temporal distribution is uneven, with both engineering-induced water scarcity and resource-based water scarcity coexisting [8,9]. This leads to a significant imbalance between water supply and ecological, domestic, and production demands, while the system's own regulatory and buffering capacity remains relatively limited. Such constraints render the regional hydrological and ecological environment generally fragile, with slow recovery processes after damage and a limited ability to resist external disturbances [10]. Studies indicate that vegetation cover on the QTP has shown an overall improving trend in recent years. However, this improvement is not spatially uniform, and human activities may cause vegetation reduction in certain localized areas. Sun et al. [11] pointed out that human activities have led to vegetation reduction in meadow zone. Xu and Wu [12] demonstrated a close correlation between vegetation and climate change. Ji et al. [13] reported that permafrost active layer deepening, driven by climate warming, leads to changes in surface hydrological connectivity and water storage capacity. These changes, in turn, influence vegetation's ability to take up water. However, studies on the temporal prediction of vegetation change processes in this region remain relatively limited, particularly in terms of systematic prediction and analysis under future scenarios.

The Normalized Difference Vegetation Index (NDVI) is commonly used as an indicator of vegetation response to climate change. Zhou et al. [14] utilized NDVI to assess vegetation responses to snow cover changes. Wu et al. [15] analyzed the response relationships between vegetation and climatic factors. Bao et al. [16] evaluated the response of vegetation dynamics to climate change in Mongolia. In addition to detecting the contribution of climatic factors to vegetation change based on historical data, researchers have also focused on the spatiotemporal dynamics of vegetation under future climate scenarios. Vasilakos et al. [17] predicted vegetation dynamics in the Mediterranean region using Long Short-Term Memory (LSTM) networks. Xu et al. [18] employed spatial autocorrelation and non-local attention networks to predict NDVI at a monthly scale. Sitch et al. [19] introduced a mechanistic model for estimating vegetation conditions. So far, studies on NDVI prediction have largely emphasized linear relationships between NDVI and driving factors. Yet the association between NDVI and components of hydrological processes is often nonlinear [20,21]. Another issue is that traditional mechanistic models, in order to improve NDVI simulation accuracy, usually need to set many parameters when describing the complex linkages between vegetation and hydrology. This approach not only makes the modeling process more complicated but also faces frequent limitations due to the availability of regional data [22]. Therefore, a balanced NDVI prediction model is a

needed one that can capture nonlinear relationships while remaining parsimonious and regionally applicable.

Among machine learning approaches, Extreme Gradient Boosting (XGBoost) has been widely used in various ecological and hydrological prediction studies [19–21]. By integrating multiple decision trees with a gradient boosting mechanism, XGBoost effectively captures complex nonlinear relationships among variables [23]. After tuning, it demonstrates high predictive accuracy and generalization ability. However, XGBoost alone functions as a "black box", it provides predictions but does not explain which input features drive the predictions or how. This limitation hinders mechanistic understanding of vegetation–hydrology interactions. This study overcomes this by combining XGBoost with SHapley Additive exPlanations (SHAP), which uses game theory to measure how much each input feature contributes to the model's predictions [24]. The SHAP analysis allows us to (i) rank the importance of multiple hydrological factors, (ii) reveal nonlinear and threshold effects, and (iii) interpret interaction patterns among drivers. To our knowledge, this framework has rarely been applied to long-term NDVI prediction and driver attribution on the QTP.

Beyond historical analysis, projecting future vegetation dynamics under different climate scenarios is essential for adaptive ecosystem management. The Coupled Model Intercomparison Project Phase 6 (CMIP6) provides standardized future climate projections under Shared Socioeconomic Pathways (SSPs), including the medium-emission (SSP2-4.5) and the high-emission (SSP5-8.5) [25,26]. While CMIP6 data have been widely used for climate change impact assessments, their integration with machine learning-based vegetation prediction models remains underexplored, especially for the QTP [27,28]. Thus, this study builds a novel analytical pipeline that combines XGBoost, SHAP, and CMIP6 scenarios. This integrated approach directly addresses the research gap: existing studies lack a systematic, interpretable, and future-oriented framework that captures nonlinear vegetation–hydrology responses on the QTP.

A critical aspect of our model is the selection of hydrological and climatic drivers. Based on the QTP's eco-hydrological characteristics and data availability, this study includes six variables [29,30] that collectively represent the region's hydrothermal conditions: precipitation (PRE), potential evapotranspiration (PE), soil moisture (SM), near-surface air temperature (NSAT), near-surface wind speed (NSWS), and relative humidity (RH). These six factors directly influence plant water availability, energy balance, and atmospheric demand. They are also the core variables provided by CMIP6 for future scenario analysis, enabling consistent historical to future modeling [31]. The justification for selecting these six variables is further elaborated in the Methods section (Section 2.2).

Therefore, this study selects the highly climate-sensitive QTP as the research area. The goal is to identify how vegetation dynamics evolve in space and time, what drives them, and how they will likely develop in the future. The main objectives are: (1) to assess historical spatiotemporal changes in vegetation dynamics; (2) to identify potential drivers of vegetation dynamics; and (3) to project long-term vegetation trends under different SSP scenarios. The research findings can provide scientific basis and decision-making support for maintaining the ecological barrier function, adaptive ecosystem management, and regional sustainable development of the QTP.

2. Materials and Methods

2.1. Study Area

The Qinghai-Tibetan Plateau (for China) is located in southwestern China (26°00′–39°47′ N, 73°19′–104°47′ E), with an average elevation exceeding 4000 m [32]. It is known as the "Roof of the World" and the "Water Tower of Asia," and is the world's largest

and highest plateau (Figure 1a). Its geographical extent stretches from the Pamir Plateau in the west to the Hengduan Mountains in the east, and from the Kunlun and Qilian Mountains in the north to the Himalayas in the south, covering a total area of approximately 2.5×10^6 km^2 [33]. This area includes the entire Tibet Autonomous Region and Qinghai Province, as well as parts of Sichuan, Yunnan, Gansu, and Xinjiang provinces. The region experiences a cold and arid climate with intense solar radiation. The annual average temperature decreases from southeast to northwest. The annual precipitation is highly unevenly distributed [34], showing a spatial pattern that gradually declines from the humid southeastern areas to the arid northwestern areas. The QTP hosts diverse ecosystem types, including alpine meadows, alpine steppes, alpine deserts, shrubs, and forests. The multi-year average NDVI of the QTP is shown in Figure 1b. Vegetation growth is constrained by multiple factors such as temperature, moisture, and radiation, making it highly sensitive to environmental changes. The QTP serves as a critical ecological security barrier for China and the world because it is the source of many major Asian rivers, hosts unique and vulnerable ecosystems, and plays an essential role in regional climate regulation [35]. Its ecological condition directly affects water security, disaster risk, and environmental stability over large downstream areas [36].

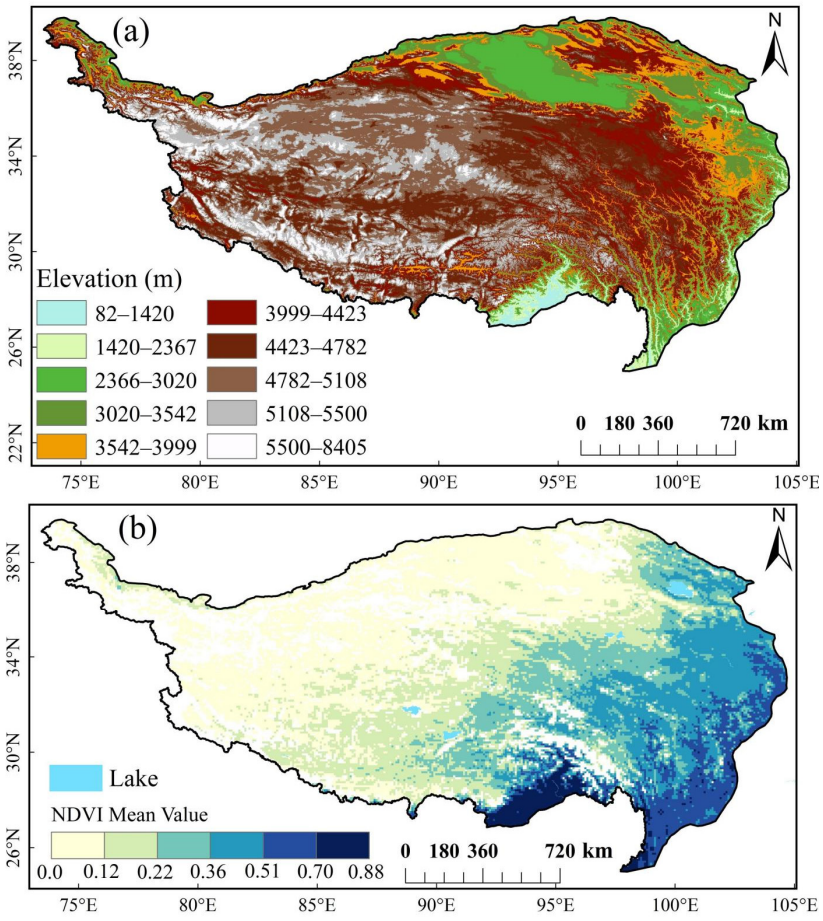


Figure 1. Study area ((**a**) elevation and (**b**) mean NDVI).

The QTP is the source of several major Asian rivers, such as the Yangtze, Yellow, Lancang, and Yarlung Tsangpo rivers. Its hydrological processes profoundly impact the water security and ecological balance of hundreds of millions of people downstream. Climate warming and more intensive human activities have, in recent years, led to increasingly pronounced glacier retreat, permafrost degradation, and changes in the spatiotemporal distribution of water resources. These changes have had profound effects on the structure

and function of vegetation ecosystems [37]. Therefore, the QTP serves as a natural laboratory for studying vegetation dynamics and adaptation mechanisms under global change, holding significant scientific research value and ecological strategic importance.

2.2. Data Sources

The data utilized in this study include historical and future data of vegetation and hydrological process elements from 1982 to 2022. The Global Inventory Modeling and Mapping Studies Normalized Difference Vegetation Index 3rd generation (GIMMS NDVI3g) is a global long-term vegetation index dataset led by the National Aeronautics and Space Administration (NASA), generated based on Advanced Very High Resolution Radiometer (AVHRR) sensor data, covering the period 1982–2022 with a spatial resolution of approximately 8 km and a temporal resolution of 15 days [38,39]. This dataset is widely used in studies on vegetation dynamics and climate change responses at global and regional scales [40,41]. In this study, this dataset is used to analyze the spatiotemporal evolution of vegetation cover in the study area and to train the prediction model.

Climate and hydrological variables are sourced from the CRU dataset released by the Climatic Research Unit (CRU) at the University of East Anglia, UK, and from ECMWF ReAnalysis 5th generation (ERA5) [42]. Both datasets are widely applied in hydrometeorological research [43,44]. The CRU dataset is a high-resolution global gridded climate data product generated through the spatial interpolation of global meteorological station observations, covering the period from 1901 to the present with a spatial resolution of $0.5^\circ \times 0.5^\circ$. This study extracts monthly precipitation (PRE), potential evapotranspiration (PE), and near-surface air temperature (NSAT) data from it to quantify regional wet/dry conditions, water balance, and ecohydrological processes, serving as key input variables for the prediction model. Near-surface wind speed (NSWS) and relative humidity (RH) data are sourced from ERA5, covering the period 1950–2022 with a spatial resolution of $0.1^\circ \times 0.1^\circ$. In this study, these datasets are used to analyze the potential driving factors and to train the prediction model.

The European Space Agency (ESA) Climate Change Initiative Soil Moisture dataset (ESA CCI SM) integrates multi-source microwave remote sensing observations, providing global surface soil moisture (SM) data at daily/monthly scales since 1978, with an original spatial resolution of $0.25^\circ \times 0.25^\circ$ [45,46]. This dataset is widely used in climate change studies, hydrological modeling, and drought monitoring. In this study, these datasets are used to analyze the potential driving factors and to train the prediction model. Key data information regarding driving factors and vegetation dynamics are summarized in Table 1.

Table 1. Key information on the driving factors and vegetation dynamics data.

Number	Variable Name	Abbreviation	Unit	Spatial & Temporal Resolution	Sources
1	Normalized Difference Vegetation Index	NDVI	/	8 km & 15 day	National Aeronautics and Space Administration (NASA)
2	Potential evapotranspiration	PE	mm	0.5° & 1 month	Climatic Research Unit (CRU)
3	Soil moisture	SM	%	0.25° & 1 month	ESA Climate Change Initiative Soil Moisture dataset (ESA CCI SM)
4	Precipitation	PRE	mm	0.5° & 1 month	Climatic Research Unit (CRU)
5	Near-surface wind speed	NSWS	m/s	0.1° & 1 month	ERA5
6	Relative humidity	RH	%	0.1° & 1 month	ERA5
7	Near-surface air temperature	NSAT	°C	0.5° & 1 month	Climatic Research Unit (CRU)

The Coupled Model Intercomparison Project Phase 6 (CMIP6) is a global climate model comparison framework coordinated by the World Climate Research Programme (WCRP), integrating nearly 100 climate system models from institutions worldwide. Under standardized experimental protocols, CMIP6 has enhanced the comparability and rigor of simulations. Compared to its predecessor CMIP5, CMIP6 demonstrates significant improvements in model physics, spatial resolution, and the representation of SSP [47,48]. The SSP2-4.5 and SSP5-8.5 scenarios, which correspond to radiative forcing levels of 4.5 W/m^{-2} and 8.5 W/m^{-2} by 2100, represent medium and high greenhouse-gas-emission pathways, respectively. This study selects multi-model outputs under the SSP2-4.5 and SSP5-8.5 scenarios (Table 2) to evaluate the response thresholds of vegetation to climate change in the study area through multi-model ensembles (MMEs).

Table 2. List of CMIP6 models applied in this study.

Number	Model Name	Institute	Land-Surface Model	Spatial Resolution (Lon. × Lat.)
1	ACCESS-CM2	CSIRO (Australia)	CABLE2.4	1.875° × 1.25°
2	ACCESS-ESM1-5	CSIRO (Australia)	CABLE2.5	1.875° × 1.25°
3	CMCC-ESM2	CMCC (Italy)	CLM4.5	1.25° × 0.94°
4	CanESM5	CCCMA (Canada)	CLASS3.6-CTEM1.2	2.8° × 2.8°
5	EC-Earth3	EC-Earth-Consortium (Europe)	HTESSEL	0.7° × 0.7°
6	GFDL-CM4	GFDL (USA)	LM4.0	1.25° × 1°
7	INM-CM4-8	INM (Russia)	INM-LND1	2° × 1.5°
8	INM-CM5-0	INM (Russia)	INM-LND2	2° × 1.5°
9	IPSL-CM6A-LR	IPSL (France)	ORCHIDEE v2	2.5° × 1.25°
10	KACE-1-0-G	KIOST (Korea)	LM3.0	1.875° × 1.25°
11	MIROC6	CCSR (Japan)	MATSIRO	1.4° × 1.4°
12	MPI-ESM1-2-HR	MPI (Germany)	CABLE2.4	0.9° × 0.9°
13	MPI-ESM1-2-LR	MPI (Germany)	CABLE2.5	1.875° × 1.875°
14	MRI-ESM2-0	MRI (Japan)	HAL 1.0	1.125° × 1.125°
15	NorESM2-LM	NCC (Norway)	CLM5	2.5° × 1.9°
16	NorESM2-MM	NCC (Norway)	CLM6	1.25° × 0.9°

Six driving factors were selected: PRE, PE, SM, NSAT, NSWS, and RH. This selection is grounded on three considerations. (1) Hydrothermal process mechanism: the six factors collectively represent water availability (PRE, SM, RH), atmospheric evaporative demand (PE), thermal energy input (NSAT), and turbulent exchange intensity (NSWS). (2) Regional specificity on the QTP: despite SM and PRE being confirmed as dominant drivers [12,49], the other factors exhibit nonlinear interactions with water conditions and could be important in certain sub-regions or seasons [29,30]. (3) Data consistency for historical and future modeling: all six variables are core outputs of CMIP6 models under SSP scenarios, ensuring comparable input sets for both historical training (1982–2022) and future projection (to 2100). All datasets were resampled to a uniform resolution of 0.5° × 0.5° using bilinear interpolation, thereby maintaining spatial consistency. Compared with the nearest neighbor interpolation, bilinear interpolation better preserves the spatial gradient characteristics of continuous variables and significantly reduces resampling errors. Although it slightly smooths extreme values, its overall accuracy is higher, making it a more suitable choice for this study [50].

2.3. Methods

2.3.1. Running Slope Difference

The running slope difference (RSD) method is a spatial statistical approach used to quantify the intensity and direction of local trend changes in time series [51–53]. Its primary

purpose is to capture the spatiotemporal heterogeneity of vegetation dynamics. The core principle of this method involves calculating local linear trends using a sliding window technique and identifying trend shifts by comparing slope differences across different periods or under varying conditions. By evaluating how the rate of change (i.e., slope) evolves over time, this method can effectively distinguish between stable, accelerating, decelerating, or reversing trends [51,54].

In this study, RSD is applied to compare the spatiotemporal differences in vegetation greening/browning trends between historical (observed) and future (projected) NDVI time series. By analyzing slope differences across sliding windows, RSD captures the intensity of trend shifts (e.g., acceleration, deceleration, or reversal) and their spatial patterns, thereby revealing the response mechanisms of vegetation dynamics to hydrological process elements.

Based on long-term vegetation data, and following the method of Li et al. [54], vegetation trend shifts are categorized into the following four types. Greening with no trend shift (GS): The entire time series shows no statistically significant directional change (slope difference fails to reject the null hypothesis of no trend change). Greening to browning (GB): An initial greening trend (positive slope) is followed by a subsequent browning trend (negative slope), indicating a reversal in vegetation growth. Greening slowing (GS): Greening continues throughout the period, but the rate of increase (slope) is lower in the later stage compared to the earlier stage. Greening accelerating (GA): The greening rate in the later period is higher than (or equal to) that in the earlier period, reflecting an intensifying greening trend. The moving window technique is employed to detect trend shifts. The study period was partitioned into sequential sub-periods, and the linear trend slope for each sub-period was computed using Ordinary Least Squares. A shift point was identified where the difference between the slopes of adjacent segments is statistically significant. For the detailed calculation process, please refer to Li et al. [54].

2.3.2. Analysis of Potential Driving Factors

To deeply investigate the potential driving factors of vegetation dynamics and their complex nonlinear statistical relationships, an interpretable machine learning analytical framework is developed herein, which couples the XGBoost (v1.7.6) model and the SHAP approach [55,56]. This framework takes vegetation dynamics as the response variable and incorporates hydrological process factors, aiming to systematically evaluate the relative importance and functional patterns of each factor in model predictions, thereby providing data-driven insights for understanding vegetation dynamic changes.

First, the XGBoost model is employed to model vegetation dynamics. XGBoost is capable of effectively capturing the nonlinear relationships and high-order interaction effects between multiple driving factors and vegetation, making it well-suited for addressing vegetation dynamics characterized by high-dimensional variables and complex factor coupling [57,58]. Through model training, key driving variables that significantly influence vegetation dynamics can be identified while fully accounting for the synergistic effects of multiple factors, thereby providing a reliable statistical foundation for subsequent mechanistic interpretation. Subsequently, the SHAP method is introduced to conduct an interpretable analysis of the model results, quantifying the contribution of each driving factor in the model's decision-making and exploring their potential functional forms [59,60]. The SHAP method is based on the concept of Shapley values from game theory, decomposing the model's prediction results into the marginal contributions of each input feature, expressed as:

$$f(x) = \phi_0 + \sum_{j=1}^{M} \phi_j(x) \quad (1)$$

where ***f(x)*** represents the model's prediction of vegetation dynamics for sample ***x***; ϕ_0 denotes the average prediction across all samples (baseline value), characterizing the baseline level of vegetation change in the absence of feature information; M is the number of driving factors; and $\phi_j(x)$ indicates the contribution of the ***j***-th feature to the vegetation dynamics prediction for sample ***x***. The SHAP value of an individual driving factor can be further expressed as:

$$\phi_j(x) = \sum_{S \subseteq F \setminus \{j\}} \frac{|S|!(M-|S|-1)!}{M!} \left[f\left(x_{S \cup \{j\}}\right) - f(x_S) \right] \quad (2)$$

where ***F*** is the set of all input features; ***S*** is any subset of ***F*** that does not include feature ***j***; $|S|$ is the number of features in subset; $f\left(x_{S \cup \{j\}}\right)$ represents the model's prediction when including feature j and subset ***S***; ***f(x)*** denotes the model's prediction when only subset S is included; and $|S|!(M-|S|-1)!/M!$ is the weight coefficient corresponding to subset ***S***. "!" denotes the factorial operation. The notation $S \subseteq F \setminus \{j\}$ represents any subset of features drawn from the full feature set ***F*** after excluding feature ***j***; the summation runs over all such subsets that do not contain feature ***j***. This expression ensures that the contributions of different driving factors in the model's predictions are quantified fairly and consistently.

Specifically, regarding the criteria for defining variable importance, we have clarified that global feature importance is determined by calculating the mean absolute SHAP values ($|\phi_j|$) for each feature across all samples. A higher mean $|\phi_j|$ indicates a greater contribution of that variable to the model's predictions, thereby establishing its relative importance concerning NDVI variations. By analyzing the global statistical characteristics of SHAP values, the dominant factors identified by the model as driving vegetation dynamics can be recognized. Through local-scale analysis, the nonlinear, non-monotonic association patterns between specific driving factors and vegetation dynamics responses. These model-based findings can outline potential key pathways of vegetation dynamics, thereby providing important clues and quantitative references for subsequent research on the physical-process-based driving mechanisms of vegetation dynamics.

2.3.3. The Prediction Model

XGBoost (Extreme Gradient Boosting) is a highly efficient ensemble algorithm that leverages gradient-boosted decision trees [57,58]. It effectively handles high-dimensional features and complex nonlinear relationships through iterative optimization, demonstrating superior performance in hydrological prediction [19–21]. In this study, the XGBoost regression model is employed to predict vegetation dynamics, with NDVI as the response variable. Predictor variables include PRE, PE, SM, NSWS, RH and NSAT.

The model was trained using observational data from 1982 to 2015, with hyperparameters optimized through grid search and five-fold cross-validation. The optimized hyperparameters included the learning rate (eta), maximum tree depth, number of boosting iterations, and regularization coefficients (lambda, alpha). Generalization ability of the model was evaluated using an independent test set (2016–2022 data). Quantification of prediction accuracy relied on R^2 and RMSE. Subsequent application of the trained model enabled projection of future vegetation dynamics under different CMIP6 scenarios.

2.3.4. Model Evaluation Metrics

To evaluate the predictive capability of the XGBoost model. The normalized root mean square error (RMSE), standard deviation (SD), and correlation coefficient (R^2) were used to quantify the deviation between predicted and observed NDVI. RMSE measures the average absolute deviation between predictions and observations, with lower values indicating a better fit [61]. SD reflects the dispersion of the predicted values around their mean, with

smaller values indicating higher stability in the model's predictions [62]. The correlation coefficient reflects the strength and direction of the linear relationship between predicted and observed values, with values closer to 1 or −1 indicating higher agreement [62].

For the CMIP6 MME, a Taylor diagram was introduced to visually compare the consistency between model simulations and reference data across three dimensions [63]: the correlation coefficient (reflecting the strength of the linear association), SD (reflecting the matching of variability), and RMSE (reflecting overall error). The Taylor diagram can reflect the relative performance of different models in capturing the spatiotemporal patterns of hydrological process elements, thereby providing a basis for model selection.

2.3.5. Research Framework

A comprehensive analytical framework was established in this study for investigating vegetation dynamics in the context of climate change (Figure 2). This study consisted of three interconnected components: Data Inputs, Analytical Methods, and Outputs and Results. First, the study collected multi-source data, including historical vegetation observations (GIMMS NDVI3g), environmental variables, and future climate projection. Second, it employed a suite of advanced analytical techniques: the running slope difference method to identify trend types and turning points, XGBoost to build a high-precision predictive model that captures non-linear climate–vegetation relationships, and SHAP analysis to quantify marginal contributions and interpret the underlying mechanisms. Finally, the framework generated outputs including the characterization of historical vegetation changes, the attribution of key driving factors, and the simulation of future NDVI responses under different scenarios.

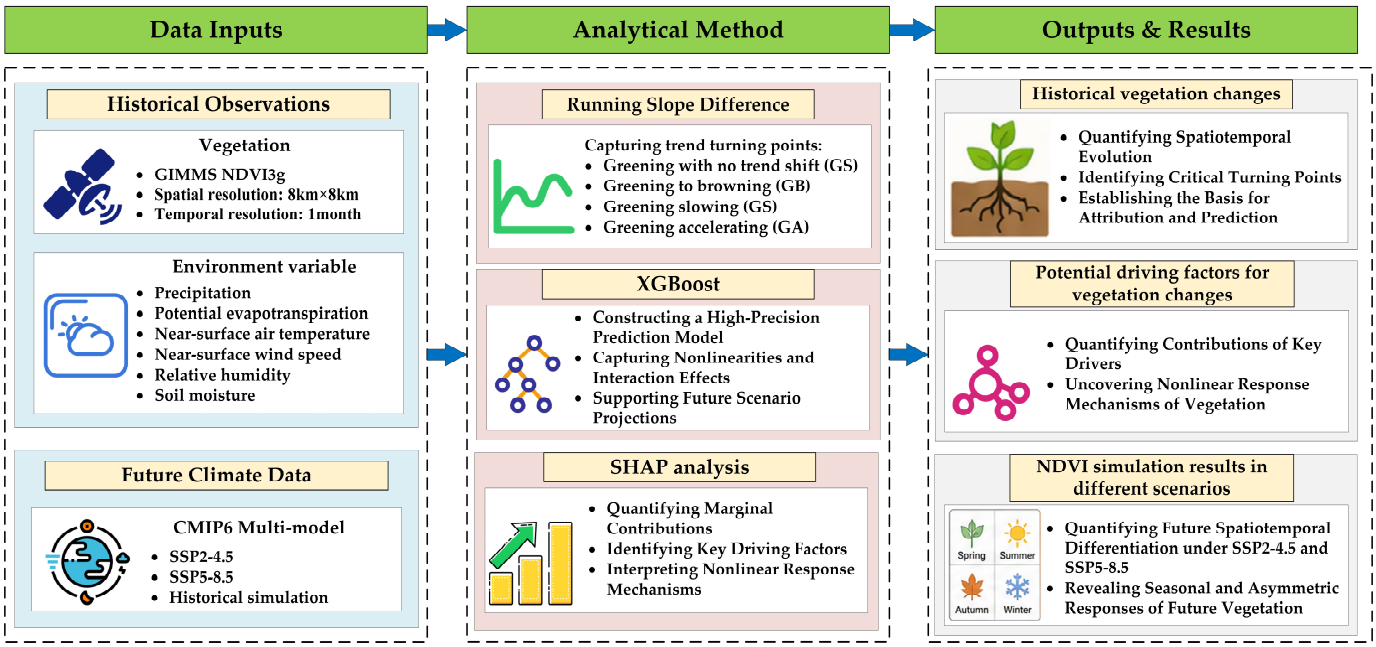


Figure 2. Conceptual and framework diagram of this study.

In this study, MATLAB software (version R2024b) was primarily used for data preprocessing, model construction, and numerical analysis. ArcGIS software (version 10.6) was employed to generate spatial distribution maps. Origin software (version 2023b) was utilized to create statistical plots.

3. Results

3.1. Historical Vegetation Changes on the QTP

This study utilized the RSD method to analyze the variation trends of vegetation on the QTP. Figure 3a displays the spatial distribution of greening trend change types. Overall, the NS characteristic on the QTP was predominantly concentrated in the western and southeastern regions, the GB characteristic was mainly distributed in the west, the GS characteristic covered a relatively small area, primarily in localized parts of the southwest and northeast, and the GA characteristic was concentrated mainly in the northeast. To illustrate the turning points in vegetation dynamic trends, Figure 3b shows the year intervals during which vegetation dynamics underwent transitions. The transition intervals of 1986–1991 and 1992–1996 were mainly concentrated in the southwest. The 1997–2001 interval was primarily distributed in the northwest and southeast. The 2002–2006 interval was more widespread, covering mainly the west, north, and southeast. The 2007–2011 interval was concentrated in the west and north. The 2012–2017 interval was distributed in small parts of the western region.

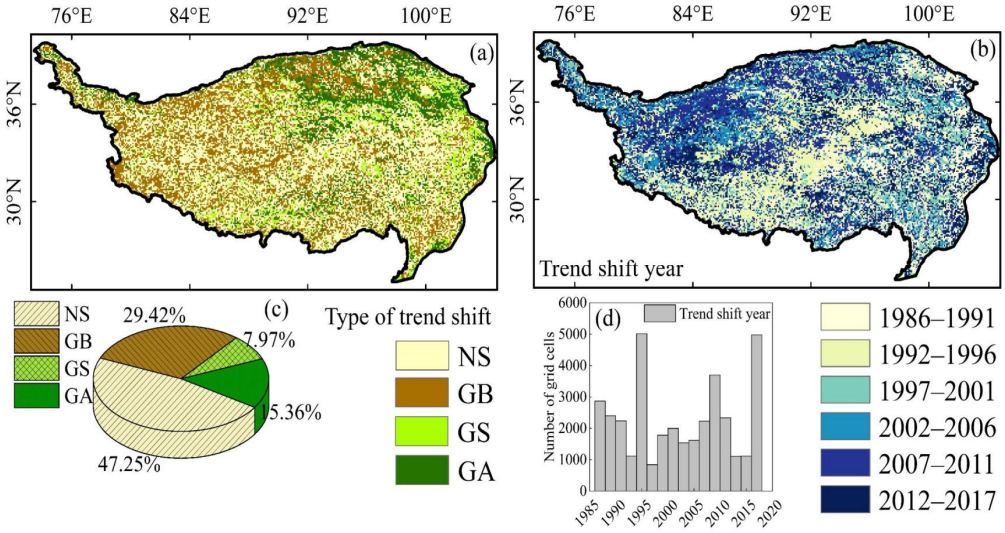


Figure 3. Spatial distribution of (**a**) greening trend shifts types; (**b**) greening trend optimal split point across QTP; (**c**) the proportions of NS, GB, GS and GA; (**d**) the number of grid cells for the turning points. (NS: Greening with no trend shift; GB: greening to browning; GS: greening slowing; GA: greening accelerating).

On the QTP, 47.25% of the area was dominated by the NS characteristic, 29.42% exhibited GB, 7.97% showed GS, and 15.36% displayed GA (Figure 3c). Overall, the predominant type of vegetation dynamic change on the QTP was NS, indicating a significant overall improvement in vegetation greenness within the region. GB also accounted for a relatively large proportion, suggesting degradation in vegetation greenness in the western regions. The turning points for the GB characteristic mainly occurred between 2007 and 2011 (Figure 3d).

3.2. Potential Driving Factors for Vegetation Changes

This study employed SHAP analysis to identify the main factors influencing vegetation dynamics, including PRE, PE, SM, NSWS, RH and NSAT. Figure 4 illustrates the impacts of these different factors on vegetation dynamics in QTP. The two most influential factors on vegetation dynamics in QTP are SM and PRE. SM had the highest mean SHAP value, indicating its strongest explanatory power for vegetation dynamics. PRE followed as the second most influential factor. The contributions of NSWS, RH, NSAT, and PE decreased

sequentially. This suggests that in the QTP ecosystem, water availability (SM, PRE) is the most critical limiting factor for vegetation growth, with its importance significantly surpassing that of thermal and atmospheric conditions.

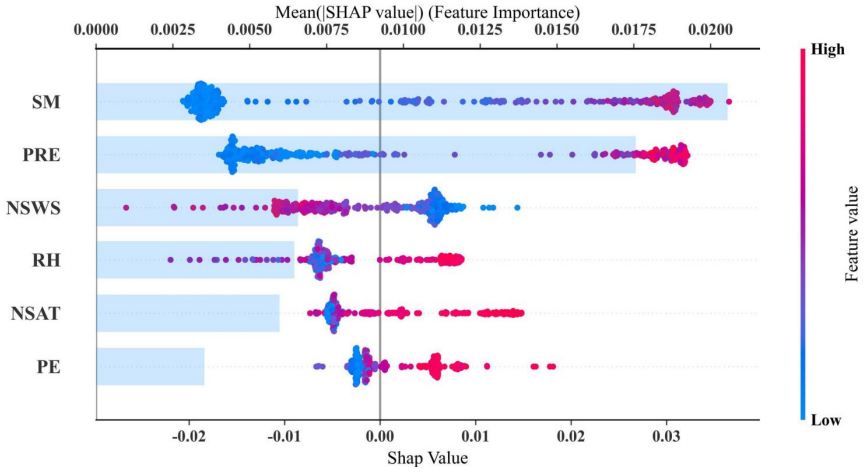


Figure 4. Feature importance and global SHAP summary plots of vegetation dynamics in QTP. (PRE: precipitation, PE: potential evapotranspiration, SM: soil moisture, NSWS: near-surface wind speed, RH: relative humidity, NSAT: near-surface air temperature).

Figure 5 reveals the complex nonlinear responses and multi-factor coupling mechanisms of various factors affecting NDVI through SHAP dependence analysis. SM shows a clear positive association with NDVI, but its promoting effect exhibits a pattern of initial strengthening followed by a slowdown as moisture increases. The influence of PRE displays distinct stage-dependent characteristics. In the lower range, its impact is weak or even negative. But beyond a certain threshold, the promoting effect increases significantly and becomes more pronounced under humid atmospheric conditions. The promoting effect of NSAT on NDVI is strongly dependent on moisture conditions. Under ample precipitation, warming shows a significant positive impact on vegetation growth. In contrast, under arid conditions, the same degree of warming may exert an inhibitory effect. Similarly, the effects of PE and NSWS are highly dependent on the SM background. When moisture is sufficient, variations in these two factors have limited impact on vegetation. However, under moisture-limited conditions, higher PE or NSWS can intensify their inhibitory effects by exacerbating water stress. These interactions highlight the multi-factor synergistic regulatory nature of vegetation dynamics on the QTP, indicating that the ecological effect of any single factor must be evaluated within the overall context of regional hydrothermal conditions.

3.3. CMIP6 Model Performance Evaluation

Based on the Taylor diagram, a comprehensive evaluation of CMIP6 models for six variables over the QTP (as shown in Figure 6) indicates that model performance exhibits significant variable dependency. For PRE, PE, and SM, most models demonstrate relatively high simulation consistency. The correlation coefficients are generally above 0.7, SD align well with observations, and RMSE values are relatively small. However, for NSAT, NSWS, and RH, model performance varies considerably. The correlation coefficients are mostly below 0.7. The SD of some models (e.g., KACE-1-0-G) deviate noticeably from observations, and RMSE values are significantly larger. This suggests that although some models can reasonably represent hydrological process variables, individual models struggle to simultaneously achieve high correlation, reasonable variability, and low error for moisture-related variables.

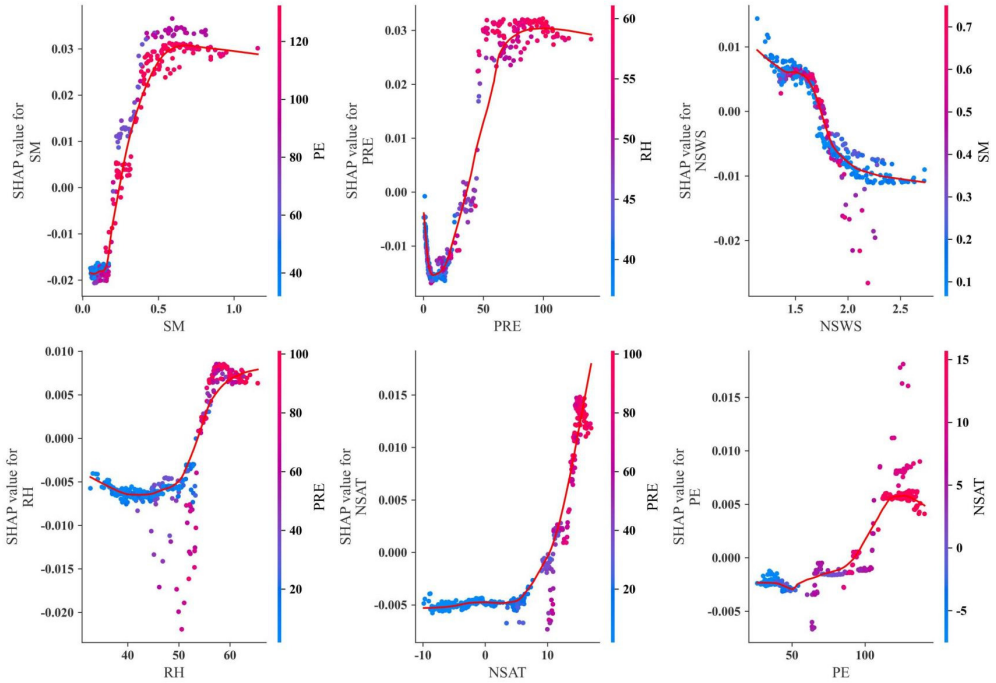


Figure 5. SHAP feature-dependence plots for vegetation dynamics in QTP. (PRE: precipitation, PE: potential evapotranspiration, SM: soil moisture, NSWS: near-surface wind speed, RH: relative humidity, NSAT: near-surface air temperature).

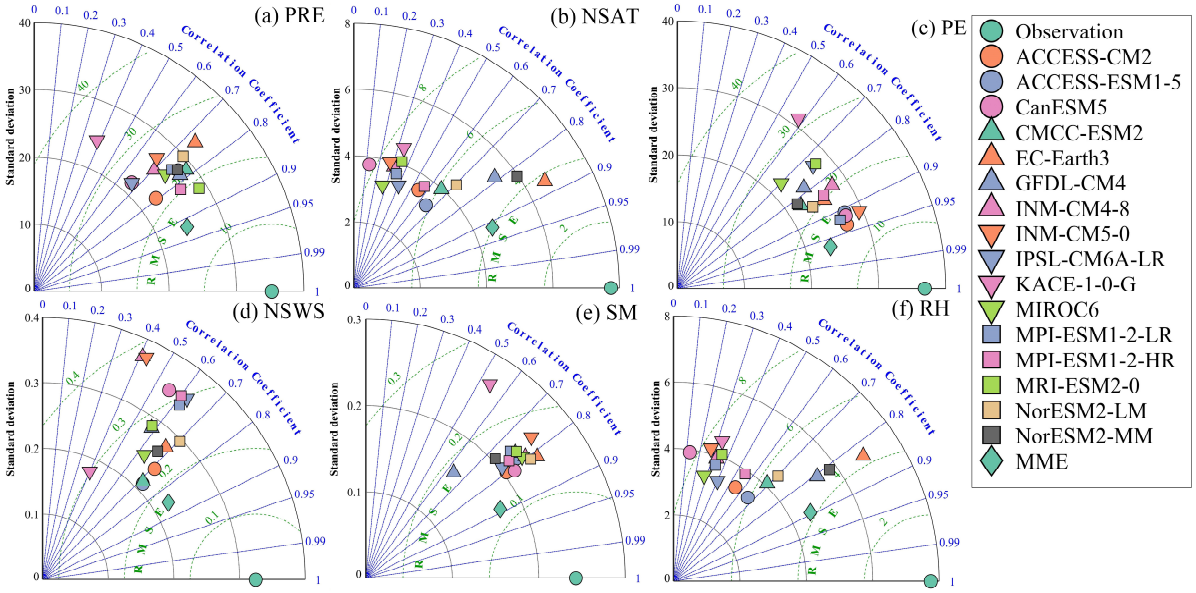


Figure 6. Taylor diagram-based evaluation of the simulation performance for predictor variables (**a**) PRE, (**b**) NSAT, (**c**) PE, (**d**) NSWS, (**e**) SM and (**f**) RH.

In this context, adopting an MME is a scientifically sound and necessary choice. The MME demonstrates comprehensive robustness superior to most individual models across all variables. For PRE and SM, the MME achieves the smallest RMSE and the best-matched SD relative to observations, while also ranking high in terms of correlation coefficients within the model group. For variables like PE, NSWS, and RH, the MME maintains an above-average performance level. By integrating complementary information from multiple models, the MME effectively offsets systematic biases and random errors inherent in individual models, significantly reducing uncertainties in climate forcing data.

Figure 7 shows the RMSE and R^2 between the NDVI predicted by the XGBoost model based on MME data and the observed values. As seen in Figure 7a, the errors exhibit regional heterogeneity, with RMSE values concentrated in the range of 0.002–0.06 for most grid cells. However, errors increase significantly along the eastern and southern margin areas. All R^2 values in Figure 7b exceed 0.6, indicating a generally strong performance. The even higher values in the eastern and southern regions further demonstrate the model's skill in reproducing NDVI variability there. In contrast, R^2 is slightly lower in the western region but remains at an above-average level, indicating that the model provides a sound explanatory power for the changes in NDVI. Most grid cells have $R^2 > 0.7$, with values primarily concentrated in the 0.6–0.8 range, reflecting the high reliability and consistency of the model's NDVI predictions.

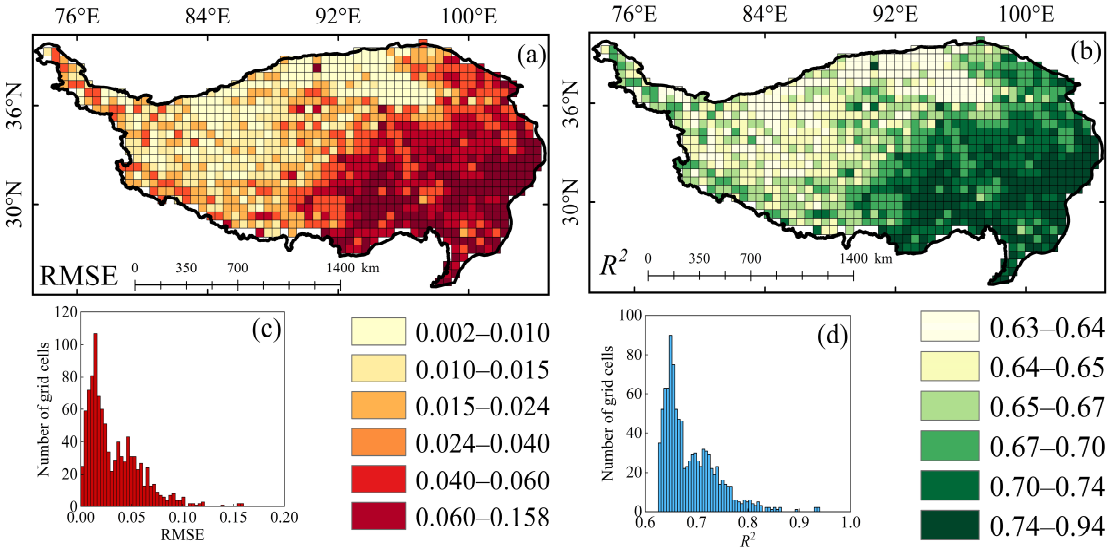


Figure 7. (**a**) Spatial pattern of RMSE across QTP. (**b**) Spatial pattern of R^2 across QTP. (**c**) The statistics of RMSE. (**d**) The statistics of R^2.

The XGBoost model based on an MME demonstrates excellent performance in predicting NDVI over the QTP. Spatially, the overall error is well-controlled with a high goodness of fit, and only localized complex regions show slightly increased errors. Statistically, errors are concentrated in the low range, and a large proportion of grid cells exhibit high R^2 values. This validates the model's capability to capture the spatiotemporal variations in NDVI, providing reliable support for regional ecological monitoring and prediction.

3.4. NDVI Simulation Results in Different Scenarios

3.4.1. Future Seasonal Changes in Vegetation

Considering China's carbon neutrality targets, this study selects 2060 as the breakpoint for future time periods, dividing them into the mid-term (2030–2060) and long-term (2061–2100). Figures 8–11 show the spatial distribution of NDVI change characteristics across different seasons on the QTP under SSP2-4.5 and SSP5-8.5 scenarios. Table 3 shows the summary table of NDVI change degree in different condition. As shown in Figure 8, during the mid-term under the SSP2-4.5 scenario (Figure 8a), the regional average NDVI change is 11.9%, with positive changes predominantly in the eastern and southern regions (increases of 5%–60%) and negative or weakly positive changes in the western and northern regions (decreases or low increases). Under the SSP5-8.5 scenario (Figure 8b), the regional average change is 17.8%, and the spatial distribution pattern is similar to that under SSP2-4.5 scenario. During the long-term under the SSP2-4.5 scenario (Figure 8c), the regional average change is 10.0%, showing a slight decrease compared to the mid-term, but

the eastern region still maintains relatively high positive changes that exceed those in the mid-term. Under the SSP5-8.5 scenario (Figure 8d), the regional average change is 26.4%, with positive changes expanding across the entire region. The western region shifts from negative to positive changes or shows a significant reduction in declines, while the increase in the eastern region becomes more pronounced.

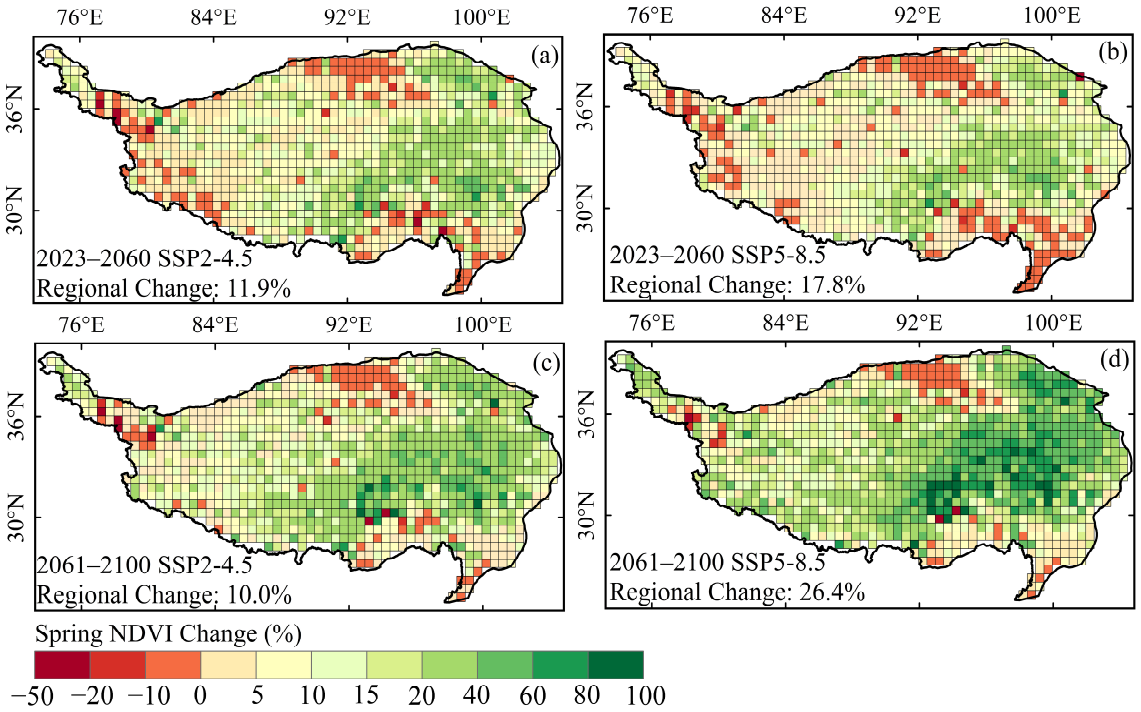


Figure 8. Spatial pattern of NDVI change degree across QTP during 2023–2060 ((**a**). SSP2-4.5 scenario; (**b**). SSP5-8.5 scenario) and 2061–2100 ((**c**). SSP2-4.5 scenario; (**d**). SSP5-8.5 scenario) in spring.

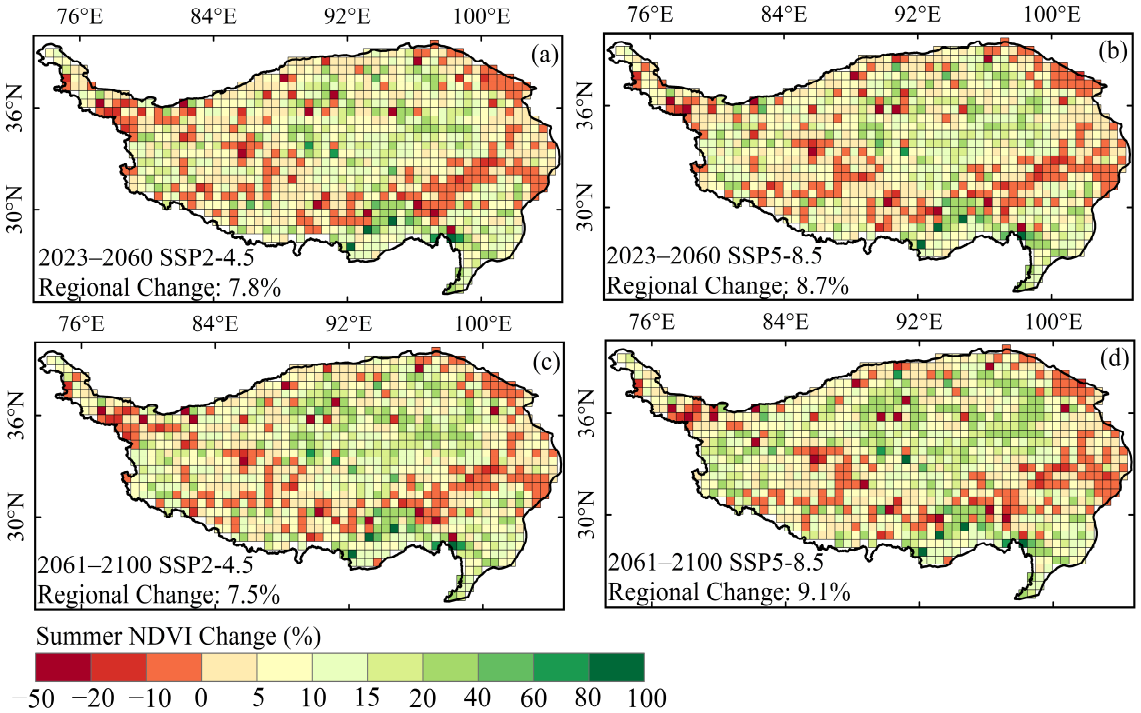


Figure 9. Spatial pattern of NDVI change degree across QTP during 2023–2060 ((**a**). SSP2-4.5 scenario; (**b**). SSP5-8.5 scenario) and 2061–2100 ((**c**). SSP2-4.5 scenario; (**d**). SSP5-8.5 scenario) in summer.

In summer, during the mid-term under the SSP2-4.5 scenario (Figure 9a and Table 3), the regional average NDVI change is 7.8%, with positive changes predominantly observed in the eastern and southern regions (increases of 5%–40%). The negative or weakly positive changes are noted in the western and northern regions. Under the SSP5-8.5 scenario (Figure 9b and Table 3), the regional average change is 8.7%, and the spatial distribution pattern resembles that under SSP2-4.5, with a slight expansion in the extent of positive changes. In the long-term, under the SSP2-4.5 scenario (Figure 9c and Table 3), the regional average change is 7.5%. Under the SSP5-8.5 scenario (Figure 9d and Table 3), the regional average change increases to 9.1%. A slight increase in positive changes.

In autumn, during the mid-term under SSP2-4.5 scenario (Figure 10a and Table 3), the regional average NDVI change is only 0.7%, but spatial variations exist. Parts of the eastern and central regions show negative changes, most of the western region exhibits slight positive changes, and the southeastern region experiences more substantial positive changes. Under the SSP5-8.5 scenario (Figure 10b and Table 3), the regional average change is 3.9%, with a spatial distribution similar to the mid-term, and no significant greening trend is observed overall. In the long-term, under the SSP2-4.5 scenario (Figure 10c and Table 3), the regional average change is 1.0%, negative changes were slightly lessened in the eastern area yet continued unabated in the western area indicating that the ecosystem tends toward stability without marked improvement. Under the SSP5-8.5 scenario (Figure 10d and Table 3), the regional average change is 11.5%, with the range of positive changes notably expanding. Although negative changes in the western region shrink, they are not completely reversed.

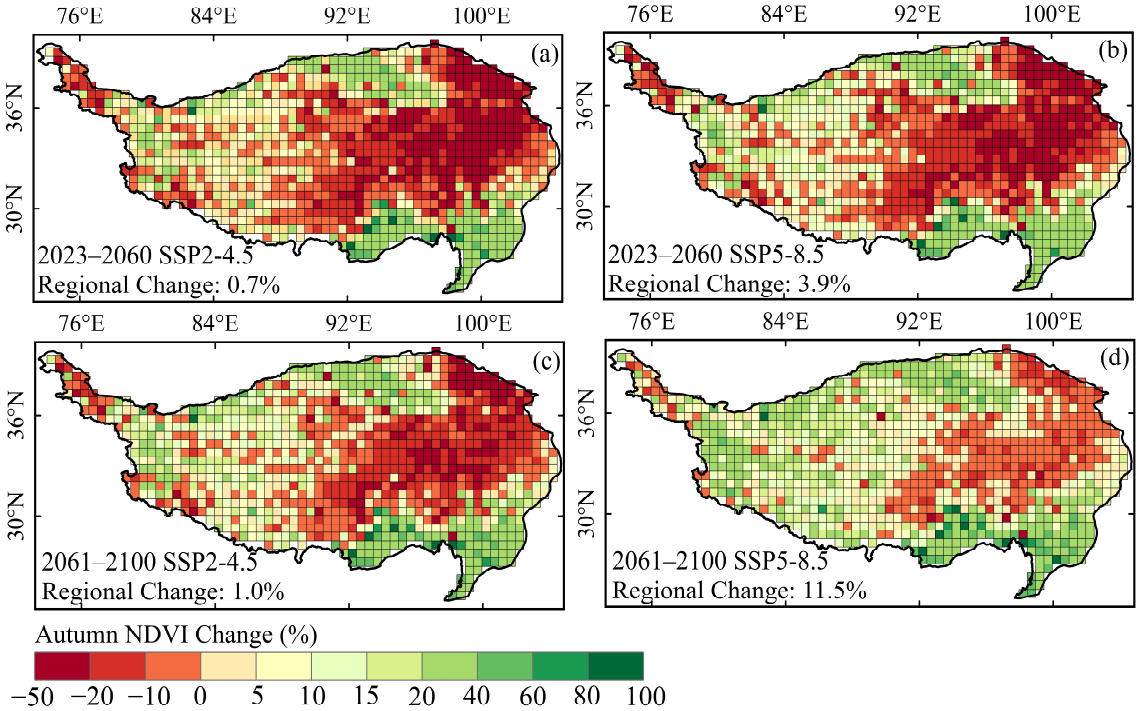


Figure 10. Spatial pattern of NDVI change degree across QTP during 2023–2060 ((**a**). SSP2-4.5 scenario; (**b**). SSP5-8.5 scenario) and 2061–2100 ((**c**). SSP2-4.5 scenario; (**d**). SSP5-8.5 scenario) in autumn.

In winter, during the mid-term under SSP2-4.5 scenario (Figure 11a and Table 3), the regional average NDVI change is 6.2%. However, there are differences in spatial distribution. Parts of the eastern and southwestern regions show negative changes, while most of the western region exhibits slight positive changes. Under the SSP5-8.5 scenario (Figure 11b and Table 3), the regional average change is 6.4%, and the spatial distribution is

similar to that in the mid-term. In the long-term, under the SSP2-4.5 scenario (Figure 11c and Table 3), the regional average change is 3.3%, with negative changes in the eastern region slightly alleviated. Under the SSP5-8.5 scenario (Figure 11d and Table 3), the regional average change is 5.9%, with an expansion in the range of positive changes, though areas with substantial negative changes persist in the eastern and southeastern regions.

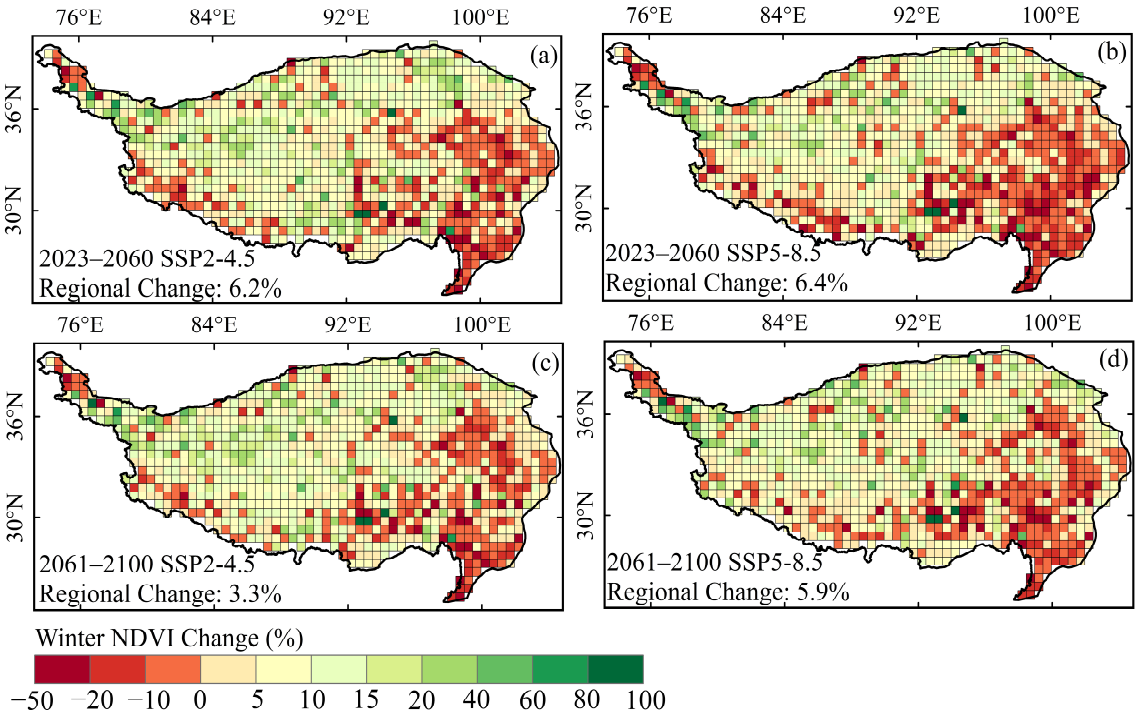


Figure 11. Spatial pattern of NDVI change degree across QTP during 2023–2060 ((**a**). SSP2-4.5 scenario; (**b**). SSP5-8.5 scenario) and 2061–2100 ((**c**). SSP2-4.5 scenario; (**d**). SSP5-8.5 scenario) in winter.

Table 3. The summary table of NDVI change degree in different conditions (unit: %).

Season	Trend	2023–2060 SSP2-4.5	2023–2060 SSP5-8.5	2061–2100 SSP2-4.5	2061–2100 SSP5-8.5
Spring	Proportion of greening areas	88.15	85.84	92.17	94.28
	Proportion of browning areas	11.85	14.16	7.83	5.72
	Regional average change	11.90	10.0	17.8	26.4
Summer	Proportion of greening areas	80.12	80.15	81.53	81.93
	Proportion of browning areas	19.88	19.85	18.47	18.07
	Regional average change	7.8	7.5	8.7	9.1
Autumn	Proportion of greening areas	46.79	47.89	53.11	72.79
	Proportion of browning areas	53.21	52.11	46.89	27.21
	Regional average change	0.7	1.0	3.9	11.5
Winter	Proportion of greening areas	73.59	66.37	75.20	72.49
	Proportion of browning areas	26.41	33.63	24.80	27.51
	Regional average change	6.2	3.3	6.4	5.9

Overall, the vegetation responses in the long-term are markedly enhanced under the high-emission scenario, reflecting an ongoing amplification of ecosystem feedback to climate warming.

3.4.2. Future Seasonal Trend of Vegetation

Figure 12 shows the NDVI trend changes under SSP2-4.5 and SSP5-8.5. As shown in Figure 12a, in spring under the SSP2-4.5 scenario, NDVI exhibits an increasing trend. Future projections show a GS shift type, indicating a weakening greening trend. Under the SSP5-8.5 scenario, NDVI shows an increasing trend. After 2060, its growth rate exceeds that under the SSP2-4.5 scenario. Future projections indicate a GA shift type, reflecting an enhanced greening trend. As shown in Figure 12b, in summer, vegetation exhibits an increasing trend under both scenarios, though the differences between the two are minimal. Future projections indicate a GS shift type. In autumn, under the SSP2-4.5 scenario, NDVI shows an increasing trend, with future projections indicating a GA shift type, reflecting an enhanced greening trend. Under the SSP5-8.5 scenario, the pattern is similar to SSP2-4.5, but the magnitude of increase is larger (Figure 12c). In winter, vegetation exhibits an increasing trend under both scenarios, though the long-term growth under SSP5-8.5 is more pronounced. Under the SSP2-4.5 scenario, future projections show a GS shift type, while under SSP5-8.5, they show a GA shift type (Figure 12d). Overall, future NDVI shows an increasing trend. Under the SSP2-4.5 scenario, the greening trend shift types for the four seasons are GS, GS, GA, and GS, respectively, while under the SSP5-8.5 scenario, the types are GA, GS, GA, and GA, respectively.

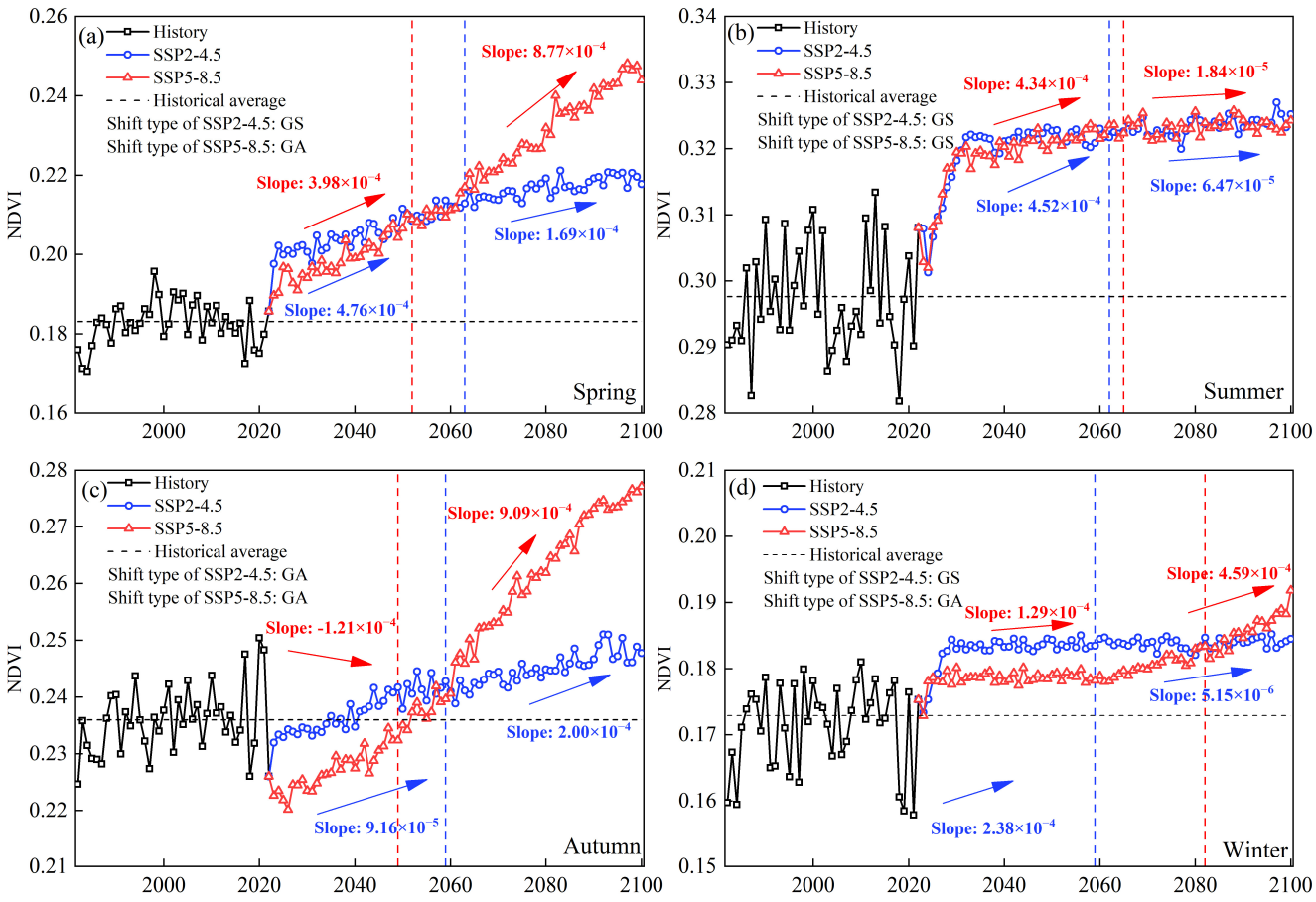


Figure 12. The change trend of NDVI and greening trend shifts types in QTP ((**a**). spring; (**b**). summer; (**c**). autumn; (**d**). winter).

4. Discussion

4.1. Historical Vegetation Changes and Nonlinear Driving Mechanisms

Consistent with the first objective of this study, our results reveal that vegetation on the QTP has experienced an overall greening trend from 1982 to 2022, but with pronounced spatiotemporal heterogeneity (Section 3.1). Approximately 47.25% of the area exhibited "greening with no trend shift (NS)", while 29.42% showed "greening to browning (GB)", 7.97% "greening slowing (GS)", and 15.36% "greening accelerating (GA)". Most turning points occurred from the late 1990s to the early 2010s, which coincides with a period of accelerated climate warming and changes in monsoon intensity [64]. Some studies have also shown that in most areas of the QTP, the vegetation is showing a trend of greening [65–67].

The seasonal and spatial patterns of future vegetation changes on the QTP reflect the spatiotemporal heterogeneity in the complex coupling between hydrothermal conditions and vegetation [68,69]. The significant greening observed in the eastern and central regions during spring may result from spring warming surpassing low-temperature thresholds, thereby advancing phenology and initiating early photosynthesis [70]. The overall weak response during summer reveals that water stress becomes the dominant limiting factor across the entire region during the peak growing season. High temperatures and strong evaporation in summer, combined with insufficient precipitation or reduced snowmelt over most parts of the QTP, make water availability the primary constraint [71]. Even with rising temperatures, it is difficult to offset the inhibitory effect of water stress on photosynthesis. Autumn shows distinct spatial heterogeneity. In the southeastern region, the lingering influence of the monsoon maintains a certain level of SM and relatively mild temperatures, and the limited extension of the growing season may lead to localized positive vegetation growth [72]. By contrast, autumn negative changes are widespread across the central and northern QTP. This largely results from growing water depletion (reduced PRE while PE remains relatively strong) as the growing season ends plus possible snow-cover harm at high elevations all of which drive a decline in productivity [73]. The winter change pattern is relatively complex. In the southeastern region, due to relatively high temperatures, winter warming significantly intensifies plant and soil respiration, which may lead to a decline in NDVI [74]. In the western high-elevation regions, the historical extreme low-temperature inhibition is partially alleviated, and reduced snow cover combined with an extended growing season supports limited physiological activity, resulting in a slight positive growth trend [14,75]. In the transitional central plateau region, winter warming is limited, and changes in snow cover and freeze–thaw processes may influence SM, leading to less pronounced changes [76,77].

The SHAP analysis (Section 3.2) identified SM and PRE as the two dominant drivers in the QTP. More importantly, the SHAP dependence plots revealed clear nonlinear and threshold effects (Figure 5). For example, SM showed a strong positive effect only above a certain threshold ($\approx$0.15 m^3 m^{-3}), below which its impact was marginal. PRE exhibited a staged pattern: a weak or even negative effect at low amounts, turning strongly positive after a threshold of about 50 mm. This indicates that the promoting effect of water on vegetation growth is not a simple linear relationship. When water availability is extremely low, a small increase in water can significantly promote vegetation growth; however, once water reaches a certain level, the marginal benefit of further increases gradually declines. Only when water exceeds a critical threshold does it become the dominant driving factor.

Apart from winter, the eastern and southeastern QTP exhibited more vigorous greening throughout all other seasons. The central and western regions, constrained by persistent water shortage, exhibited weak responses or even localized browning (GB type). These spatial patterns can be linked to permafrost distribution, elevation gradients, and monsoon influence. In the western QTP, continuous permafrost limits root water uptake and soil

hydrology. Climate warming deepens the active layer, which may initially reduce surface soil moisture [10]. In the central QTP, the weakening of the Indian summer monsoon has reduced precipitation supply over the past two decades [78]. In contrast, the eastern and southeastern margins are more influenced by the East Asian monsoon, receiving relatively stable moisture [79]. Elevation also modulates the response. High-elevation areas are more temperature-limited, while mid-elevation areas are water-limited [80,81]. The results of this study suggest that future management must consider these topographic elements and permafrost distributions, not merely broad climatic zones.

4.2. Future Vegetation Dynamics Under CMIP6 Scenarios: Uncertainties and Management Implications

This study projected NDVI changes under SSP2-4.5 and SSP5-8.5 for two future periods (2030–2060 and 2061–2100). The MME approach was used to reduce individual model biases (Section 3.3). The Taylor diagram (Figure 6) showed that MMEs outperform most single models for PRE, SM, and PE, but larger uncertainties remain for NSAT, NSWS, and RH. This variable-dependent performance is an important source of uncertainty that must be considered when interpreting future predictions. First, CMIP6 models show considerable spread in simulating PRE and NSAT over the QTP, particularly in the western high-elevation areas and during autumn and winter. The poor model agreement in these seasons introduces uncertainty into the projected water supply. Second, the XGBoost model, while skillful in capturing nonlinear relationships, inherits and may amplify input uncertainties because its predictions are sensitive to extreme values [82]. Third, the interaction effects detected by SHAP mean that joint errors in multiple variables can propagate non-additively [83]. Therefore, the projected NDVI changes in the western QTP and in autumn and winter seasons should be interpreted with greater caution than the more robust spring greening signal in the east. A number of investigations have similarly indicated that vegetation on the QTP will continue to green in the coming decades [65–67]. Future efforts should fully conduct quantitative uncertainty analysis, yet the results of this study still provide important reference value for research on the future evolution of vegetation on the QTP.

The above findings lead us to propose the following targeted strategies for ecological preservation and climate adaptation across the QTP:

Water focused management prioritizing SM and PRE. Given that SM and PRE are the dominant drivers, in water-limited central and western regions, low impact measures such as micro-basin construction, rainwater harvesting, and dry-season grazing exclusion should be implemented to enhance water retention. In contrast, in the relatively water-sufficient eastern and southeastern areas, attention should focus on preventing abrupt vegetation degradation induced by land use changes rather than water stress.

Season-specific adaptation actions. Because spring shows the highest rate of change and autumn exhibits strong internal spatial variability, early-spring ecological restoration (e.g., controlled artificial PRE enhancement in March–April) and flexible autumn grazing adjustments should be prioritized. Summer greening is relatively stable, so routine monitoring suffices. Winter responses are weak in the east and negligible in the west; thus, reducing anthropogenic disturbance in the east is recommended, while no active winter intervention is needed in the west.

Spatially differentiated strategies aligned with vegetation change characteristics. For the 47.25% of the QTP with NS characteristics, long-term baseline monitoring is sufficient. For the 29.42% with GB, policies should maintain existing favorable conditions and prevent tipping points. For the 7.97% with GS, accelerated restoration measures (e.g., seeding native species, soil stabilization) should be applied following the shift point (late 1990s–early

2010s). For the 15.36% with GA, real time adaptive management and early warning systems are necessary.

Scenario-dependent planning for future pathways. Under the medium-emission SSP2-4.5 scenario, current adaptive measures may be largely adequate. However, under the high-emission SSP5-8.5 scenario, the projected stronger responses in spring and autumn and the amplified spatial differences require additional investments in water storage infrastructure and flexible seasonal grazing policies to cope with increased hydroclimatic variability and degradation risks in vulnerable zones.

4.3. Limitation and Prospects

Several limitations should be acknowledged. First, uncertainties in climate forcing data remain substantial. Although this study used an MME to average out systematic biases, errors in PRE, SM, and especially NSAT and RH over complex terrain are unavoidable [45]. Second, our model did not explicitly account for topography and land-surface heterogeneity, such as slope aspect, permafrost thaw dynamics, and soil texture [84], which are known to modulate water and heat fluxes on the QTP [85]. Third, the NDVI data themselves have inherent limitations, including saturation in dense vegetation and sensitivity to snow cover, soil background, and atmospheric conditions—particularly problematic in winter and over high-elevation barren areas [86]. Fourth, we did not include human activities (grazing intensity, land-use change, ecological restoration projects) as drivers [87], which may lead to attribution biases in regions with significant anthropogenic influence.

Future research should prioritize: (i) integrating higher-resolution climate reanalysis and topographic correction to better capture local hydrothermal gradients; (ii) developing hybrid models that couple machine learning with process-based representations of permafrost hydrology, phenology, and carbon-nitrogen cycles; (iii) quantifying the combined effects of climate change and human activities (e.g., grazing exclusion, wetland drainage) using causal inference methods; and (iv) improving the detection of vegetation response thresholds through extended observation networks and field experiments. By addressing these limitations, future studies can provide more robust, actionable guidance for safeguarding the QTP's ecological security under rapid global change.

5. Conclusions

A systematic evaluation was performed on the spatiotemporal characteristics of QTP vegetation greening from 1982 to 2022, along with a quantitative analysis of its key climatic drivers and projections of future vegetation dynamics under different climate scenarios. The main conclusions are summarized as follows:

A greening trend has been observed in QTP vegetation across the recent 40-year period. But with evident spatiotemporal shifts. Approximately 47.25% of the QTP is dominated by the NS characteristic, 29.42% exhibits GB, 7.97% shows GS, and 15.36% displays GA. Most greening shift points occurred from the late 1990s to the early 2010s.

SM and PRE are the two factors contributing most to NDVI changes, with their importance exceeding that of NSAT, NSWS, RH and PE. Significant nonlinear relationships exist between the driving factors and NDVI.

Vegetation responses to climate forcing on the QTP vary by season and region. Responses are stronger in spring and autumn, relatively moderate in summer, and show clear spatial differences between the eastern and western parts of the QTP in winter. The eastern and southeastern parts of the QTP exhibit more active greening trends across all seasons except winter. The central and western regions, constrained by water availability, show weak responses or even localized degradation. High-emission scenarios amplify these differences.

To conclude, the complexity of future QTP vegetation responses to climate change lies in their nonlinear interactions and threshold effects, wherein water availability (SM and PRE) emerges as the dominant control. Future ecological conservation and climate change adaptation strategies for the QTP should therefore adopt a zone-specific and season-specific approach for precise adaptation and management. For example, in the eastern and southeastern regions, management should focus on maintaining growing season carbon sinks and preventing non-growing season carbon loss under winter warming; in the central and western water-limited regions, drought resilient measures and water conservation are priorities. Under the high-emission SSP5-8.5 scenario, the amplified seasonal and spatial differences call for stronger interventions, particularly in spring and autumn when vegetation responses are most pronounced. The present study delivers both significant insights into alpine ecosystem responses to global change and essential scientific underpinning for preserving the integrity of the QTP ecological security barrier and elevating its climate resilience.

Author Contributions: Conceptualization, Q.M., P.C. and Q.H.; data curation, J.L.; formal analysis, Q.M. and W.Y.; investigation, P.C. and Z.Z.; methodology, Q.M.; resources, Q.H. and P.C.; software, Q.M.; validation, Z.Z., X.W. and Q.M.; writing—original draft, Q.M., X.W. and Q.H.; writing—review and editing, W.Y., Q.H., and P.C. All authors have read and agreed to the published version of the manuscript.

Funding: This study was funded by the General Program of the 2024 Xizang Autonomous Region Natural Science Foundation, grant number XZ202401ZR0109, Linzhi City University-Local Cooperation Project, grant number XDHZ-2025-06, 2024 Xizang Autonomous Region Science and Technology Program Project—Bases and Talent, grant number XZ202401JD0005, the Youth Fund Project of Xizang Agriculture & Animal Husbandry University, grant number NYQNZR2025-03, the Young Investigator Program of the 2024 Xizang Autonomous Region Natural Science Foundation, grant number XZ202401ZR0096, the Open Research Fund from the Research Center of Civil & Hydraulic and Power Engineering of Xizang, grant number XZ202305CHP2008B, and the Open Research Fund from the Research Center of Civil & Hydraulic and Power Engineering of Xizang, grant number XZ202305CHP2009B.

Data Availability Statement: The data presented in this study are available on request from the corresponding author.

Acknowledgments: We gratefully acknowledge the helpful and constructive comments on the manuscript provided by the editors and anonymous reviewers.

Conflicts of Interest: The authors declare that they have no known competing financial interests or personal relationships that could have appeared to influence the work reported in this paper.

References

1. Ma, B.; Zeng, W.; Hu, G.; Cao, R.; Cui, D.; Zhang, T. Normalized Difference Vegetation Index Prediction Based on the Delta Downscaling Method and Back-Propagation Artificial Neural Network under Climate Change in the Sanjiangyuan Region, China. *Ecol. Inform.* **2022**, *72*, 101883. [CrossRef]
2. Luan, J.; Ma, N. Responses of Seasonal Hydrological Processes to Vegetation Change in the Yellow River Basin. *J. Hydrol.* **2025**, *660*, 133449. [CrossRef]
3. Xiao, J.; Xie, B.; Zhou, K.; Li, W.; Liang, C.; Li, J.; Xie, J.; Zhang, X.; Pang, X. Responses of Hydrological Processes to Vegetation Greening and Climate Change in Subtropical Watersheds. *J. Hydrol. Reg. Stud.* **2024**, *55*, 101946. [CrossRef]
4. Huang, S.; Yan, H.; Zhang, C.; Wang, G.; Acquah, S.J.; Yu, J.; Li, L.; Ma, J.; Opoku Darko, R. Modeling Evapotranspiration for Cucumber Plants Based on the Shuttleworth-Wallace Model in a Venlo-Type Greenhouse. *Agric. Water Manag.* **2020**, *228*, 105861. [CrossRef]
5. Yan, H.; Zhao, S.; Zhang, C.; Zhang, J.; Wang, G.; Li, M.; Deng, S.; Liang, S.; Jiang, J. Calibration and Assessment of Evapotranspiration Methods for Cucumber Plants in a Venlo-type Greenhouse. *Irrig. Drain.* **2024**, *73*, 119–135. [CrossRef]

6. Ullah, I.; Mao, H.; Rasool, G.; Gao, H.; Javed, Q.; Sarwar, A.; Khan, M.I. Effect of Deficit Irrigation and Reduced N Fertilization on Plant Growth, Root Morphology and Water Use Efficiency of Tomato Grown in Soilless Culture. *Agronomy* **2021**, *11*, 228. [CrossRef]
7. Li, L.; Zhang, Y.; Wu, J.; Li, S.; Zhang, B.; Zu, J.; Zhang, H.; Ding, M.; Paudel, B. Increasing Sensitivity of Alpine Grasslands to Climate Variability along an Elevational Gradient on the Qinghai-Tibet Plateau. *Sci. Total Environ.* **2019**, *678*, 21–29. [CrossRef] [PubMed]
8. Fan, Y.; Fang, C. Measuring Qinghai-Tibet Plateau's Sustainability. *Sustain. Cities Soc.* **2022**, *85*, 104058. [CrossRef]
9. Liu, J.; Qin, K.; Xie, G.; Xiao, Y.; Huang, M.; Gan, S. Is the "water Tower" Reassuring? Viewing Water Security of Qinghai-Tibet Plateau from the Perspective of Ecosystem Services "Supply-Flow-Demand". *Environ. Res. Lett.* **2022**, *17*, 094043. [CrossRef]
10. Wang, S.; Guo, L.; He, B.; Lyu, Y.; Li, T. The Stability of Qinghai-Tibet Plateau Ecosystem to Climate Change. *Phys. Chem. Earth* **2020**, *115*, 102827. [CrossRef]
11. Sun, L.; Li, H.; Wang, J.; Chen, Y.; Xiong, N.; Wang, Z.; Wang, J.; Xu, J. Impacts of Climate Change and Human Activities on NDVI in the Qinghai-Tibet Plateau. *Remote Sens.* **2023**, *15*, 587. [CrossRef]
12. Xu, T.; Wu, H. Spatiotemporal Analysis of Vegetation Cover in Relation to Its Driving Forces in Qinghai-Tibet Plateau. *Forests* **2023**, *14*, 1835. [CrossRef]
13. Ji, F.; Yuan, S.; Fan, L.; Zhu, L.; Jin, J.; Yao, Y.; Liu, Y.; Guan, T.; Zheng, C.; Zhang, J. Thresholds in Land-Atmosphere Interactions on the Qinghai-Tibet Plateau: Impacts of Permafrost Degradation via Vegetation Changes. *J. Hydrol.* **2025**, *662*, 133912. [CrossRef]
14. Zhou, Y.; Liu, F.; Zhang, G.; Wang, J. Response of the Normalized Difference Vegetation Index (NDVI) to Snow Cover Changes on the Qinghai-Tibet Plateau. *Remote Sens.* **2024**, *16*, 2140. [CrossRef]
15. Wu, K.; Chen, J.; Yang, H.; Yang, Y.; Hu, Z. Spatiotemporal Variations in the Sensitivity of Vegetation Growth to Typical Climate Factors on the Qinghai-Tibet Plateau. *Remote Sens.* **2023**, *15*, 2355. [CrossRef]
16. Bao, G.; Bao, Y.; Sanjjava, A.; Qin, Z.; Zhou, Y.; Xu, G. NDVI-Indicated Long-Term Vegetation Dynamics in Mongolia and Their Response to Climate Change at Biome Scale. *Int. J. Climatol.* **2015**, *35*, 4293–4306. [CrossRef]
17. Vasilakos, C.; Tsekouras, G.; Kavroudakis, D. LSTM-Based Prediction of Mediterranean Vegetation Dynamics Using NDVI Time-Series Data. *Land* **2022**, *11*, 923. [CrossRef]
18. Xu, L.; Cai, R.; Yu, H.; Du, W.; Chen, Z.; Chen, N. Monthly NDVI Prediction Using Spatial Autocorrelation and Nonlocal Attention Networks. *IEEE J. Sel. Top. Appl. Earth Obs. Remote Sens.* **2024**, *17*, 3425–3437. [CrossRef]
19. Sitch, S.; Smith, B.; Prentice, I.; Arneth, A.; Bondeau, A.; Cramer, W.; Kaplan, J.; Levis, S.; Lucht, W.; Sykes, M.; et al. Evaluation of Ecosystem Dynamics, Plant Geography and Terrestrial Carbon Cycling in the LPJ Dynamic Global Vegetation Model. *Glob. Change Biol.* **2003**, *9*, 161–185. [CrossRef]
20. Alvarez, D.; Poveda, G. Spatiotemporal Dynamics of NDVI, Soil Moisture and ENSO in Tropical South America. *Remote Sens.* **2022**, *14*, 2521. [CrossRef]
21. Zhou, Z.; Xue, P.; Zhou, X.; Wang, T.; Ding, Y.; Zhao, Y.; Chen, P.; Wang, X. Assessing the Soil Moisture-Vegetation Mutual Feedback Relationship in Different Climatic Regions of Mainland China. *Catena* **2025**, *249*, 108684. [CrossRef]
22. Bao, Z.; Zhang, J.; Wang, G.; Guan, T.; Jin, J.; Liu, Y.; Li, M.; Ma, T. The Sensitivity of Vegetation Cover to Climate Change in Multiple Climatic Zones Using Machine Learning Algorithms. *Ecol. Indic.* **2021**, *124*, 107443. [CrossRef]
23. Li, Q.; Gao, H.; Zhang, X.; Ni, J.; Mao, H. Describing Lettuce Growth Using Morphological Features Combined with Nonlinear Models. *Agronomy* **2022**, *12*, 860. [CrossRef]
24. Mardian, J.; Champagne, C.; Bonsal, B.; Berg, A. A Machine Learning Framework for Predicting and Understanding the Canadian Drought Monitor. *Water Resour. Res.* **2023**, *59*, e2022WR033847. [CrossRef]
25. John, A.; Douville, H.; Ribes, A.; Yiou, P. Quantifying CMIP6 Model Uncertainties in Extreme Precipitation Projections. *Weather Clim. Extrem.* **2022**, *36*, 100435. [CrossRef]
26. Song, Z.; Xia, J.; She, D.; Li, L.; Hu, C.; Hong, S. Assessment of Meteorological Drought Change in the 21st Century Based on CMIP6 Multi-Model Ensemble Projections over Mainland China. *J. Hydrol.* **2021**, *601*, 126643. [CrossRef]
27. Chauhdary, J.N.; Li, H.; Akbar, N.; Javaid, M.; Rizwan, M.; Akhlaq, M. Evaluating Corn Production under Different Plant Spacings through Integrated Modeling Approach and Simulating Its Future Response under Climate Change Scenarios. *Agric. Water Manag.* **2024**, *293*, 108691. [CrossRef]
28. Zheng, Z. Winter Wheat Production on the Guanzhong Plain of Northwest China under Projected Future Climate with SimCLIM. *Agric. Water Manag.* **2020**, *239*, 106233. [CrossRef]
29. Ding, M.; Wu, H.; Lei, R.; Fan, H.; Li, J.; Li, K.; Zhu, Q.; Wan, R.; Fu, C. Riverine Isoscapes Modeling in the Yangtze River Basin, China: Insights Into Basin Processes and Source-Water Contributions. *Water Resour. Res.* **2025**, *61*, e2024WR039587. [CrossRef]
30. Wang, S.; Huang, S.; Wang, C.; Zhang, X.; Wu, J.; Gulakhmadov, A.; Niyogi, D.; Chen, N. Global Anthropogenic Effects on Meteorological—Hydrological—Soil Moisture Drought Propagation: Historical Analysis and Future Projection. *J. Hydrol.* **2025**, *653*, 132755. [CrossRef]

31. Chauhdary, J.N.; Li, H.; Ragab, R.; Rakibuzzaman, M.; Khan, A.I.; Zhao, J.; Akbar, N. Climate Change Impacts on Future Wheat (Triticum Aestivum) Yield, Growth Periods and Irrigation Requirements: A SALTMED Model Simulations Analysis. *Agronomy* **2024**, *14*, 1484. [CrossRef]
32. Chang, Y.; Ding, Y.; Zhang, S.; Zhao, Q.; Jin, Z.; Qin, J.; Shangguan, D. Quantifying the Response of Runoff to Glacier Shrinkage and Permafrost Degradation in a Typical Cryospheric Basin on the Tibetan Plateau. *Catena* **2024**, *242*, 108124. [CrossRef]
33. Zhu, Y.; Liu, S.; Wei, J.; Wu, K.; Bolch, T.; Xu, J.; Guo, W.; Jiang, Z.; Xie, F.; Yi, Y.; et al. Glacier-Level and Gridded Mass Change in River Sources in the Eastern Tibetan Plateau Region (ETPR) from the 1970s to 2000. *Earth Syst. Sci. Data* **2025**, *17*, 1851–1871. [CrossRef]
34. Liu, X.; Zhou, Q.; Ma, Y.; Zhi, Z.; Liu, R.; Ma, W. Temporal and Spatial Variation Characteristics of Precipitation Isohyets on the Qinghai-Tibet Plateau from 1961 to 2023. *Atmosphere* **2025**, *16*, 698. [CrossRef]
35. Wang, Y.; Ye, A.; Quincey, D.J.; James, W. Projected Decline in Glacier Runoff Contribution during Drought Periods across the Qinghai-Tibetan Plateau. *J. Hydrol.* **2026**, *664*, 134583. [CrossRef]
36. Wang, Y.; Xue, K.; Hu, R.; Ding, B.; Zeng, H.; Li, R.; Xu, B.; Pang, Z.; Song, X.; Li, C.; et al. Vegetation Structural Shift Tells Environmental Changes on the Tibetan Plateau over 40 Years. *Sci. Bull.* **2023**, *68*, 1928–1937. [CrossRef] [PubMed]
37. Wang, Y.; Gao, H.; Jin, H.; Xi, Q.; Wang, P.; Chen, D. Root Zone Storage Capacity Reveals Ecohydrological Turning Points in Tibetan Plateau Permafrost Regions. *Catena* **2026**, *263*, 109716. [CrossRef]
38. Ye, W.; Van Dijk, A.I.J.M.; Huete, A.; Yebra, M. Global Trends in Vegetation Seasonality in the GIMMS NDVI3g and Their Robustness. *Int. J. Appl. Earth Obs. Geoinf.* **2021**, *94*, 102238. [CrossRef]
39. Fensholt, R.; Proud, S.R. Evaluation of Earth Observation Based Global Long Term Vegetation Trends—Comparing GIMMS and MODIS Global NDVI Time Series. *Remote Sens. Environ.* **2012**, *119*, 131–147. [CrossRef]
40. Fensholt, R.; Rasmussen, K. Analysis of Trends in the Sahelian "rain-Use Efficiency" Using GIMMS NDVI, RFE and GPCP Rainfall Data. *Remote Sens. Environ.* **2011**, *115*, 438–451. [CrossRef]
41. Xiao, J.; Huang, K.; Lin, Y.; Ren, P.; Zu, J. Assessing Vegetation Phenology across Different Biomes in Temperate China-Comparing GIMMS and MODIS NDVI Datasets. *Remote Sens.* **2022**, *14*, 6180. [CrossRef]
42. Zhang, Z.; Li, P.; Wang, J. A Meteorological Data Quality Control Framework for Tea Plantations Using Association Rules Mined from ERA5 Reanalysis Data. *Agriculture* **2026**, *16*, 226. [CrossRef]
43. Ma, S.; Zhang, S.; Wang, N.; Huang, C.; Wang, X. Prolonged Duration and Increased Severity of Agricultural Droughts during 1978 to 2016 Detected by ESA CCI SM in the Humid Yunnan Province, Southwest China. *Catena* **2021**, *198*, 105036. [CrossRef]
44. Zhang, G.; Su, X.; Ayantobo, O.O.; Feng, K. Drought Monitoring and Evaluation Using ESA CCI and GLDAS-Noah Soil Moisture Datasets across China. *Theor. Appl. Climatol.* **2021**, *144*, 1407–1418. [CrossRef]
45. Zheng, C.; Jia, L.; Zhao, T. A 21-Year Dataset (2000-2020) of Gap-Free Global Daily Surface Soil Moisture at 1-Km Grid Resolution. *Sci. Data* **2023**, *10*, 139. [CrossRef]
46. Xu, H.; Sun, H.; Xu, Z.; Wang, Y.; Zhang, T.; Wu, D.; Gao, J. kNDMI: A Kernel Normalized Difference Moisture Index for Remote Sensing of Soil and Vegetation Moisture. *Remote Sens. Environ.* **2025**, *319*, 114621. [CrossRef]
47. Cook, B.; Mankin, J.; Marvel, K.; Williams, A.; Smerdon, J.; Anchukaitis, K. Twenty-First Century Drought Projections in the CMIP6 Forcing Scenarios. *Earths Future* **2020**, *8*, e2019EF001461. [CrossRef]
48. Wang, T.; Tu, X.; Singh, V.; Chen, X.; Lin, K. Global Data Assessment and Analysis of Drought Characteristics Based on CMIP6. *J. Hydrol.* **2021**, *596*, 126091. [CrossRef]
49. Zhu, B.; Tu, M.; Wang, M.; Li, G.; Sui, X.; Zhang, Z.; Chen, X. Soil Moisture Constraints Override Atmospheric Aridity in Governing Vegetation Dynamics on the Warming Qinghai-Tibetan Plateau. *Ecol. Indic.* **2026**, *185*, 114742. [CrossRef]
50. Gebremedhin, M.; Lubczynski, M.; Maathuis, B.; Teka, D. Novel Approach to Integrate Daily Satellite Rainfall with In-Situ Rainfall, Upper Tekeze Basin, Ethiopia. *Atmos. Res.* **2021**, *248*, 105135. [CrossRef]
51. Lou, W.; Sun, C.; Zuo, B.; Dong, M.; Song, Z.; Shi, L.; He, Y.; Tong, Y. Divergent Mechanisms Drive Multi-Decadal Drought Intensification in South America: A Trend Turning Analysis from 1958 to 2023. *Int. J. Climatol.* **2026**, *46*, e70242. [CrossRef]
52. Zuo, B.; Li, J.; Sun, C.; Zhou, X. A New Statistical Method for Detecting Trend Turning. *Theor. Appl. Climatol.* **2019**, *138*, 201–213. [CrossRef]
53. Lou, W.; Sun, C.; Zuo, B. Concurrent Trend Turnings of Drought Severity across Afro-Eurasian Continent since 1950. *Glob. Planet. Change* **2024**, *243*, 104628. [CrossRef]
54. Li, H.; Liu, X.; Liu, J.; Meng, Y.; Xing, L.; Zhao, H.; Wang, C.; Wang, R.; Wang, B. Shifts in Greening Trend of Afforestation over the Loess Plateau from 2000 to 2023. *Ecol. Indic.* **2025**, *177*, 113756. [CrossRef]
55. Xue, Z.; Diao, S.; Yang, F.; Fei, L.; Wang, W.; Fang, L.; Liu, Y. Identifying Forest Drought Sensitivity Drivers in China Under Lagged and Accumulative Effects via XGBoost-SHAP. *Remote Sens.* **2025**, *17*, 2903. [CrossRef]
56. Sun, J.; Wang, L.; Huang, S.; Li, Y.; Wang, J. Study on the Lagged Response Mechanism of Vegetation Productivity under Atypical Anthropogenic Disturbances Based on XGBoost-SHAP. *Remote Sens.* **2026**, *18*, 300. [CrossRef]

57. Sokhansefat, S.; Kanani-Sadat, Y.; Nasseri, M. Modeling Vegetation Dynamics in Complex Topography under Impacts of Climate Change: Integration of Spatial Clustering and Optimized XGBoost. *J. Environ. Manag.* **2025**, *387*, 125902. [CrossRef]
58. Khosravi, Y.; Ouarda, T. A Geographically Weighted XGBoost Framework for Pixel-Level Modeling of Vegetation Responses Using Multi-Source Earth Observation Data. *ISPRS J. Photogramm. Remote Sens.* **2026**, *235*, 105–132. [CrossRef]
59. Zhang, Y.; Wang, P.; Li, Y.; Han, D.; Wu, D.; Liu, S.; Guo, J. A Quantification Method for Cumulative Drought Effects on Summer Maize Yield Incorporating Recovery Dynamics Based on Vegetation Water Index. *Agric. Water Manag.* **2025**, *320*, 109865. [CrossRef]
60. Li, T.; Wu, Y.; Ren, F.; Tian, L.; Li, M. Assessing the Impact of Stand Structure on Forest Net Primary Productivity: A Multiple Machine Learning-SHAP Models and DSEM Integrated Approach. *Comput. Electron. Agric.* **2025**, *236*, 110427. [CrossRef]
61. Hemanandhini, S.; Rajkumar, L. Performance Evaluation of CMIP6 Climate Models for Selecting a Suitable GCM for Future Precipitation at Different Places of Tamil Nadu. *Environ. Monit. Assess.* **2023**, *195*, 928. [CrossRef] [PubMed]
62. Ty, T.; Tri, L.; Tho, N.; Toan, N.; Nhat, G.; Downes, N.; Kumar, P.; Minh, H. Evaluating the Performance of CMIP6 GCMs to Simulate Precipitation and Temperature over the Vietnamese Mekong Delta. *J. Clim. Change* **2023**, *9*, 31–42. [CrossRef]
63. Zabihi, O.; Ahmadi, A. Multi-Criteria Evaluation of CMIP6 Precipitation and Temperature Simulations over Iran. *J. Hydrol. Reg. Stud.* **2024**, *52*, 101707. [CrossRef]
64. He, W.; Liu, Y.; Sun, H.; Taghizadeh-Hesary, F. How Does Climate Change Affect Rice Yield in China? *Agriculture* **2020**, *10*, 441. [CrossRef]
65. Wang, H.; Zhan, J.; Wang, C.; Liu, W.; Yang, Z.; Liu, H.; Bai, C. Greening or Browning? The Macro Variation and Drivers of Different Vegetation Types on the Qinghai-Tibetan Plateau from 2000 to 2021. *Front. Plant Sci.* **2022**, *13*, 1045290. [CrossRef]
66. Wu, J.; Li, M.; Zhang, X.; Fiedler, S.; Gao, Q.; Zhou, Y.; Cao, W.; Hassan, W.; Mărgărint, M.C.; Tarolli, P.; et al. Disentangling Climatic and Anthropogenic Contributions to Nonlinear Dynamics of Alpine Grassland Productivity on the Qinghai-Tibetan Plateau. *J. Environ. Manag.* **2021**, *281*, 111875. [CrossRef]
67. Luo, H.; Tang, Y.; Zhu, X.; Di, B.; Xu, Y. Greening Trend in Grassland of the Lhasa River Region on the Qinghai-Tibetan Plateau from 1982 to 2013. *Rangel. J.* **2016**, *38*, 591–603. [CrossRef]
68. Zhang, L.; Xin, C.; Sun, M. Temporal and Spatial Evolution of Gross Primary Productivity of Vegetation and Its Driving Factors on the Qinghai-Tibet Plateau Based on Geographical Detectors. *Atmosphere* **2025**, *16*, 940. [CrossRef]
69. Zhao, X.; Deng, H.; Wang, W.; Han, F.; Li, C.; Zhang, H.; Dai, Z. Impact of Naturally Leaking Carbon Dioxide on Soil Properties and Ecosystems in the Qinghai-Tibet Plateau. *Sci. Rep.* **2017**, *7*, 3001. [CrossRef]
70. Xu, W.; Liu, X. Response of Vegetation in the Qinghai-Tibet Plateau to Global Warming. *Chin. Geogr. Sci.* **2007**, *17*, 151–159. [CrossRef]
71. Liu, X.; Chen, Y.; Li, Z.; Li, Y.; Zhang, Q.; Zan, M. Driving Forces of the Changes in Vegetation Phenology in the Qinghai-Tibet Plateau. *Remote Sens.* **2021**, *13*, 4952. [CrossRef]
72. Wang, H.; Peng, P.; Kong, X.; Zhang, T.; Yi, G. Vegetation Dynamic Analysis Based on Multisource Remote Sensing Data in the East Margin of the Qinghai-Tibet Plateau, China. *PeerJ* **2019**, *7*, e8223. [CrossRef]
73. Tang, Y.; Chen, J.; Xu, J.; Xu, J.; Ni, J.; Zheng, Z.; Yu, B.; Wu, J.; Huang, Y. The Impact of Autumn Snowfall on Vegetation Indices and Autumn Phenology Estimation. *Remote Sens.* **2024**, *16*, 4783. [CrossRef]
74. Lou, P.; Wu, T.; Yang, S.; Wu, X.; Chen, J.; Zhu, X.; Chen, J.; Lin, X.; Li, R.; Shang, C.; et al. Deep Learning Reveals Rapid Vegetation Greening in Changing Climate from 1988 to 2018 on the Qinghai-Tibet Plateau. *Ecol. Indic.* **2023**, *148*, 110020. [CrossRef]
75. Fan, T.; Zhong, X.; Wang, C.; Zhou, L.; Zhou, Z. Phenological Shifts of Vegetation in Seasonally Frozen Ground and Permafrost Zones of the Qinghai-Tibet Plateau. *Remote Sens.* **2025**, *17*, 3391. [CrossRef]
76. Chang, J.; Wang, G.; Gao, Y.; Wang, Y. The Influence of Seasonal Snow on Soil Thermal and Water Dynamics under Different Vegetation Covers in a Permafrost Region. *J. Mt. Sci.* **2014**, *11*, 727–745. [CrossRef]
77. Man, Z.; Weng, B.; Yang, Y.; Gong, X.; Li, M.; Yu, Z. Effects of the Freezing-Thawing Cycle Mode on Alpine Vegetation in the Nagqu River Basin of the Qinghai-Tibet Plateau. *Water* **2019**, *11*, 2122. [CrossRef]
78. Li, X.; Long, D.; Scanlon, B.R.; Mann, M.E.; Li, X.; Tian, F.; Sun, Z.; Wang, G. Climate Change Threatens Terrestrial Water Storage over the Tibetan Plateau. *Nat. Clim. Change* **2022**, *12*, 801–807. [CrossRef]
79. Yang, Y.; Zhao, L.; Shen, X.; Xiao, Z.; Li, Q. The Spring Heat Source Over the Qinghai–Tibetan Plateau Linked With the Winter Warm Arctic–Cold Siberia Pattern Impacting Summer Drought in China. *Front. Earth Sci.* **2022**, *10*, 835101. [CrossRef]
80. Pepin, N.; Bradley, R.S.; Diaz, H.F.; Baraer, M.; Caceres, E.B.; Forsythe, N.; Fowler, H.; Greenwood, G.; Hashmi, M.Z.; Liu, X.D.; et al. Elevation-Dependent Warming in Mountain Regions of the World. *Nat. Clim. Change* **2015**, *5*, 424–430. [CrossRef]
81. Wang, X.; Hu, Z.; Zhang, Z.; Tang, J.; Niu, B. Altitude-Shifted Climate Variables Dominate the Drought Effects on Alpine Grasslands over the Qinghai–Tibetan Plateau. *Sustainability* **2024**, *16*, 6697. [CrossRef]
82. Begum, S.S.; Swamy, A.; Dhanka, S.; Abu-Shareha, A.A.; Khan, M.; Husain, I. Generative Adversarial Networks and Hyperparameter-Optimized XGBoost for Enhanced Heart Disease Prediction. *Sci. Rep.* **2026**, *16*, 11326. [CrossRef] [PubMed]

83. Takefuji, Y. Beyond the Black Box: Enhancing Feature Explainability in Machine Learning with SHAP and Complementary Approaches. *Comput. Electron. Agric.* **2026**, *240*, 111226. [CrossRef]
84. Solangi, K.A.; Siyal, A.A.; Wu, Y.; Abbasi, B.; Solangi, F.; Lakhiar, I.A.; Zhou, G. An Assessment of the Spatial and Temporal Distribution of Soil Salinity in Combination with Field and Satellite Data: A Case Study in Sujawal District. *Agronomy* **2019**, *9*, 869. [CrossRef]
85. Chen, H.; Good, S.P.; Zahn, E.; Bou-Zeid, E.; Caylor, K.K.; Fiorella, R.P.; Haagsma, M.; Wang, L. Shifts in Evapotranspiration Components During Heatwaves Alter Surface Cooling. *Earth's Future* **2026**, *14*, e2025EF006562. [CrossRef]
86. Xu, Y.; Ma, Y.; Cayuela, M.L.; Sánchez-Monedero, M.A.; Wang, Q. Compost Biochemical Quality Mediates Nitrogen Leaching Loss in a Greenhouse Soil under Vegetable Cultivation. *Geoderma* **2020**, *358*, 113984. [CrossRef]
87. Liu, X.; Chen, Y.; Liu, Y.; Wang, S.; Jin, J.; Zhao, Y.; Yu, D. A Framework Combining CENTURY Modeling and Chronosequences Sampling to Estimate Soil Organic Carbon Stock in an Agricultural Region with Large Land Use Change. *Agronomy* **2023**, *13*, 1055. [CrossRef]

Disclaimer/Publisher's Note: The statements, opinions and data contained in all publications are solely those of the individual author(s) and contributor(s) and not of MDPI and/or the editor(s). MDPI and/or the editor(s) disclaim responsibility for any injury to people or property resulting from any ideas, methods, instructions or products referred to in the content.